

Modulated Taylor–Couette flow

By C. F. BARENGHI AND C. A. JONES

School of Mathematics, The University, Newcastle-upon-Tyne, NE1 7RU, UK

(Received 12 September 1988)

The onset of instability in temporally modulated Taylor–Couette flow is considered. Critical Reynolds numbers have been found by computing Floquet exponents. We find that frequency modulation of the inner cylinder introduces a small destabilization, in agreement with the narrow-gap theory of Hall and some recent experiments of Ahlers. We review the previous computational literature on this problem, and find a number of contradictory results: the source of these discrepancies is examined, and a satisfactory resolution is achieved. Nonlinear axisymmetric calculations on the modulated problem have been done with an initial value code using a spectral method with collocation. The results are compared satisfactorily with Ahlers' measurements.

At low modulation frequency, a large destabilization has been observed in past experiments. We show that this cannot be explained on the basis of perfect bifurcation theory: an analysis of the modulated amplitude equation shows that very small imperfections can substantially affect the behaviour at low frequency by giving rise to 'transient' vortices at subcritical Reynolds number. We argue that these 'transient' vortices are the source of the large destabilization seen in some experiments. Modelling the imperfections in the initial-value code provides additional confirmation of this effect.

1. Introduction

The stability of flows which vary periodically in time is a problem which is receiving increasing attention. This interest has a number of causes. It arises partly from the recognition that many flows in nature are driven by periodic forces, partly from the improved experimental techniques available in fluid dynamics, and partly from the general progress in the area of dynamical systems. This has led to the investigation of the effect of time modulation on the parameters that control the onset of an instability.

Some of the major prototype problems of modulated hydrodynamics have been reviewed by Davis (1976): parallel shear flow, Bénard convection and Taylor–Couette flow. In this paper we investigate the problem of modulated Taylor–Couette flow.

Our concern is the motion of an incompressible fluid of density ρ and kinematic viscosity ν which is contained in the gap between two concentric cylinders which rotate at assigned angular velocities. We make use of the following notation: R_1 and R_2 are the radii of the inner and outer cylinder, and Ω_1 and Ω_2 are their respective angular velocities. The gap width is $d = R_2 - R_1$ and the radius ratio is $\eta = R_1/R_2$.

We distinguish between a 'steady' and a 'modulated' Taylor–Couette flow. In the 'steady' Taylor–Couette problem the velocities of the inner and the outer cylinders are kept constant: let us assume for simplicity that the outer cylinder is fixed ($\Omega_2 = 0$) and that the inner cylinder rotates at angular velocity Ω_1 . If Ω_1 is small

enough then the motion of the fluid around the inner cylinder is purely azimuthal and it is called Couette flow. If Ω_1 is larger than a critical velocity Ω_{10} then the Couette flow is unstable: a secondary flow onsets with non-zero values of the radial and axial velocity components; this new flow, called Taylor-vortex flow, is in the form of axisymmetric vortices stacked on top of each other in the axial direction. A similar transition from azimuthal Couette flow to Taylor-vortex flow holds in the more general case in which both Ω_1 and Ω_2 are not zero, although if the cylinders rotate in opposite directions a direct transition to a non-axisymmetric state is possible. Further instabilities of the Taylor vortex flow at higher velocity and the onset of time-dependent non-axisymmetric flow are not our concern at this stage.

In modulated Taylor–Couette flow we address the question of what happens if the velocities of the inner and the outer cylinders are not constant but vary periodically in time at given frequency and amplitude. We consider a modulation of the form

$$\left. \begin{aligned} \Omega_1 &= \bar{\Omega}_1(1 + \epsilon_1 \sin(\omega_1 t)), \\ \Omega_2 &= \bar{\Omega}_2(1 + \epsilon_2 \sin(\omega_2 t)). \end{aligned} \right\} \quad (1.1)$$

It is apparent that by a proper choice of the many parameters in (1.1) a great number of interesting flows can be produced. Riley & Laurence (1976) and Carmi & Tustaniwskyj (1981) investigated theoretically modulations both with zero mean velocities and with non-zero mean velocities. In particular they studied the modulation of the inner cylinder around zero mean with fixed outer cylinder; this case has an interesting limit when the outer cylinder is absent, which has been considered from both the theoretical and experimental point of view by Seminara & Hall (1976, 1977), and then by Park, Barenghi & Donnelly (1980) in an experiment in which they found spatial subharmonic bifurcations. What happens in the case described by (1.1) at large modulation amplitudes was studied by both Riley & Laurence (1976) and Carmi & Tustaniwskyj (1981), and more recently by Kuhlmann, Roth & Lücke (1989), who discovered subharmonic response when the flow becomes supercritical in both rotation directions during a cycle.

In the present paper we want to concentrate our attention on simpler situations, in which the basic flow is a standard Couette flow, and the modulation is a perturbation superimposed on it; our motivation is that some important questions about the effect of modulation at low frequency and low amplitude near the steady vortex flow threshold are not yet understood.

The first case of modulated Taylor–Couette flow which we study is when the outer cylinder is fixed and the inner cylinder is modulated around a non-zero mean

$$\left. \begin{aligned} \Omega_1(t) &= \bar{\Omega}_1(1 + \epsilon_1 \sin(\omega_1 t)), \\ \Omega_2(t) &= 0. \end{aligned} \right\} \quad (1.2)$$

We assume that the amplitude of the modulation is such that the inner cylinder always rotates in the same direction more or less rapidly, i.e. $\epsilon_1 < 1$. Now if $\bar{\Omega}_1$ is sufficiently small, the flow is azimuthal and the inner cylinder is an oscillating boundary from which a damped viscous wave originates and penetrates into the fluid as far as a Stokes layer thickness $\delta_s = (2\nu/\omega_1)^{1/2}$. If $\bar{\Omega}_1$ is higher than a critical value $\bar{\Omega}_{1c}$ a vortex flow onsets. The question which then naturally arises is whether the modulation makes the flow more or less stable to the onset of vortices than in the steady case. This leads to the introduction of the threshold shift parameter $r = (\bar{\Omega}_{1c} - \Omega_{10})/\Omega_{10}$, and to the study of how the threshold shift varies as a function of modulation amplitude ϵ_1 and modulation frequency ω_1 . In particular one expects

interesting things to happen at frequencies for which the Stokes layer has size comparable with the gap between the cylinders: at high frequency only a thin layer of fluid close to the inner cylinder is affected by the oscillatory motion on top of the average rotation $\bar{\Omega}_1$ and the modulation produces a less significant influence.

A useful measure of the frequency of modulation is the parameter $\gamma_1 = (\omega_1 d^2/2\nu)^{\frac{1}{2}}$ which is the gap width d divided by the Stokes-layer thickness δ_s . From now on we shall use the symbol ω_1 to denote the angular frequency of modulation in dimensionless units, based on the viscous time d^2/ν ; thus we have $\omega_1 = 2\gamma_1^2$.

The pioneering work done on the subject of modulated Taylor–Couette flow, which stimulated the whole field of modulated hydrodynamics, was the experiment of Donnelly: (Donnelly, Reif & Suhl 1962; Donnelly 1964). Donnelly found that, for given ϵ_1 and ω_1 , the critical velocity $\bar{\Omega}_{1c}$ at which modulated vortex flow onsets is larger than the velocity Ω_{10} of the onset of steady Taylor vortices. In his definition of $\bar{\Omega}_{1c}$ it was assumed that above $\bar{\Omega}_{1c}$ the vortices have amplitude with the dependence $A^2 = \bar{\Omega}_1 - \bar{\Omega}_{1c}$, where A is an axial or radial velocity component, in analogy to what happens in the steady Taylor–Couette problem. However, at velocities less than $\bar{\Omega}_{1c}$ Donnelly observed vortices which appear and disappear during a cycle, which he called ‘transient vortices’.

Hall (1975) calculated the onset of modulated vortex flow in the case of narrow gap ($\eta \rightarrow 1$) in both the limits of high and low frequency. In the low-frequency limit he used an expansion in both small modulation amplitude and small frequency of modulation. He discovered that the lowest correction to the onset of vortices in the steady problem is negative and of the order ϵ_1^2 , i.e. the modulation weakly destabilizes the flow. More precisely he found that the critical Taylor number of modulated vortex flow $Ta_c = 2\bar{\Omega}_{1c}^2 R_1 d^3/\nu^2$ is a series of the form

$$Ta_c = Ta_0 - 208.6 \epsilon_1^2 + 1.7 \epsilon_1^2 \omega_1^2 + O(\epsilon_1^4, \epsilon_1^2 \omega_1^4). \quad (1.3)$$

Here $Ta_0 = 3389.9$ is the critical Taylor number for the onset of steady vortex flow in the narrow-gap limit and $\alpha = 3.1266$ is the critical dimensionless wavenumber (the axial wavenumber in units of the gap width). Note that the series (1.3) has terms with alternating sign and it probably converges slowly; in the same paper Hall also added that the next contribution in (1.3) is the term $-1300 \epsilon_1^4$. The nonlinear behaviour was also studied by Hall (1975, 1983) who derived a differential equation in time for the amplitude of the disturbance: this amplitude equation will be discussed in §3.

Riley & Laurence (1976) developed a numerical code to study the stability of the viscous wave using Floquet theory and a Galerkin expansion, again in the narrow-gap limit. As mentioned above, these authors considered several choices of parameters in (1.1). In the case of modulation of the inner cylinder around non-zero mean, which is our concern, they confirmed Hall’s result that low-frequency modulation destabilizes the flow.

The extension of the theory to the case of finite radius ratio was carried out by Carmi & Tustaniwskyj (1981) who developed a numerical implementation of Floquet theory and studied a variety of choices of parameters. For the case described by (1.2) they considered two values of the radius ratio, $\eta = 0.957$ and $\eta = 0.693$. At amplitude $\epsilon_1 = 0.5$ for both values of η they found that the modulation has a strong destabilizing effect in the low-frequency limit. The authors claimed that the flow becomes unstable at low frequency as soon as the peak velocity during a cycle $\bar{\Omega}_1(1 + \epsilon_1)$ is equal to the velocity of the onset of steady vortices Ω_{10} , in agreement with a similar experimental observation of Thompson (1969). Carmi & Tustaniwskyj also argued that in Riley & Laurence’s calculation there is an approximation which

is not justified in unsteady flows and that this is probably the origin of their mutual disagreement. In a following paper Tustaniwskyj & Carmi (1980) developed an energy stability theory and confirmed the work of Carmi & Tustaniwskyj (1981).

Kuhlmann (1985) developed a model equation for modulated Taylor–Couette flow in the narrow-gap limit by mode truncation of the Navier–Stokes equations and the introduction of simpler modified boundary conditions. He found that the model was satisfactory for the case of steady Taylor flow; however, in the case of modulation it predicted stabilization at all frequencies instead of destabilization. It was found that mode truncation rather than the modified boundary conditions was responsible and that the inclusion of more modes restored the destabilization. A similar model of mode truncation was also derived by Hsieh & Chen (1984) in the steady case and by Bhattacharjee, Banerjee & Kumar (1986) in the modulated case: the calculation of the latter produced destabilization at low frequency, in agreement with the theory of Hall, but disagreed with Hall at higher frequency by exhibiting stabilization.

Walsh & Donnelly (1988*a*) performed experiments at different values of the radius ratio. At the lowest frequencies of modulation they found large negative threshold shifts, of the same order of magnitude as Carmi & Tustaniwskyj's: for example at $\eta = 0.88$, $\epsilon_1 = 0.5$ and $\omega_1 = 0.5$ they measured $r \approx -28\%$. However, the shape of Carmi & Tustaniwskyj's stability boundary was not in agreement with Walsh & Donnelly's: the former showed large destabilization over a wide range in frequency, while the latter presented small threshold shifts with a sudden increase of the destabilization only below a critical frequency, for example $\omega_1 < 4$ at $\epsilon_1 = 0.5$ and $\eta = 0.88$.

G. Ahlers (1988, private communication) performed a series of experiments at $\eta = 0.75$ which showed only a small destabilization. For example at $\epsilon_1 = 0.5$ and $\omega_1 = 4$ he found $r = -3\%$ only, more in agreement with the theory of Hall than that of Carmi & Tustaniwskyj. Ahlers also did laser-Doppler measurements of a component of the flow velocity at a fixed point as a function of time and obtained characteristic non-harmonic profiles.

While our work was in progress we received a preprint from Kuhlmann *et al.* In this paper they developed both a finite-difference numerical simulation of the Navier–Stokes equations at radius ratio $\eta = 0.65$ and an analytic Galerkin approximation with four modes. They found that the modulation weakly destabilizes the flow at low frequency, in agreement with Hall and in disagreement with Carmi & Tustaniwskyj. They also studied large-amplitude modulation, as mentioned above, and discussed the differences and the similarities between Taylor–Couette flow and Bénard convection when subjected to external periodic driving.

We conclude from this summary that there is a disagreement in the literature about whether a low-frequency modulation produces a large destabilizing effect, $r = O(\epsilon_1)$, or rather a small destabilizing effect, $r = O(\epsilon_1^2)$. In particular, in support of the former claim there is the numerical work of Carmi & Tustaniwskyj (1981) with the successive work of Tustaniwskyj & Carmi (1980) and the experiments of Thompson (1969) and Walsh & Donnelly (1988*a*); in support of the latter claim there are the results of the different theories of Hall (1975), Riley & Laurence (1977) and Kuhlmann *et al.* (1988) together with the experiments of Ahlers (1988).

In order to try to resolve the disagreement between these two claims we have developed both an initial-value code to study modulated Taylor–Couette flow and a linear Floquet theory to study the onset of vortices. These numerical tools are briefly described in §2. Our findings about the onset of vortex flow, which we present and compare with the existing theories and experiments in §4, are that the modulation

produces only a small negative threshold shift, in agreement with the claim of weak destabilization.

This does not explain, however, why so many investigations, including recent experimental work, have found large destabilization at low frequency. In §3 we show that small imperfections in the apparatus have a large effect at low frequency, and we identify some physical mechanisms which could lead to suitable imperfections. These imperfections do not cause very significant effects in the steady problem, but they have important consequences in time-dependent flows close to threshold. We present evidence which suggests that the discrepancies in the literature are primarily due to imperfections.

The effect of imperfections has been studied in the context of the convection of a horizontal layer of fluid confined by lateral walls. If the walls are not perfect insulators, which is the case in all experiments, then the bifurcation to the convective state is not perfect: there is a smooth transition from conduction to finite convective amplitude; see, for example, Daniels (1977) and Hall & Walton (1979). These authors found that the differential equation for the amplitude contains an extra constant forcing term due to the heat leaking through the lateral walls.

Ahlers *et al.* (1981) and then Cross, Hohenberg & Lücke (1983) studied the effect of both a step and a linear ramp of the heat current on the onset of convection and were able to explain the experimental data by making use of a forcing term in the amplitude equation. These authors also included a stochastic force with Gaussian white noise into the model so as to simulate mechanical vibrations, random motion and thermal noise. Finally Ahlers, Hohenberg & Lücke (1985*a*) studied the case of modulated thermal convection: they used a truncation of the Boussinesq equations which led to a three-mode model; the model is a generalization of the Lorenz model to the case of external modulation. They found that the imperfection, which is due to heat leaking through the lateral walls, leads to a time-dependent forcing term in the Lorenz equations, which can be solved numerically. This approach was used to make a quantitative analysis of experimental data both by Ahlers, Hohenberg & Lücke (1985*b*) and by Niemela & Donnelly (1987).

In §3 we discuss imperfections in the modulated Taylor–Couette system by means of the amplitude equation (Hall 1975, 1983), modified by including a constant term. The amplitude equation with imperfections is also used in §4, alongside the numerical solutions of the Navier–Stokes equations, and quantitative comparison with experiments is presented.

Until now we have discussed modulated Taylor–Couette flow described by assigning the angular velocities (1.2). There is another simple situation which we consider, for which again the basic flow is of the Couette type and the modulation is a perturbation on top of it. In this second situation the inner cylinder rotates at constant angular velocity and the outer cylinder is modulated around zero mean:

$$\left. \begin{aligned} \Omega_1(t) &= \bar{\Omega}_1, \\ \Omega_2(t) &= \epsilon_2 \bar{\Omega}_1 \sin(\omega_2 t). \end{aligned} \right\} \quad (1.4)$$

This case has been the subject of a recent experiment by Walsh & Donnelly (1988*b*). They rotated the inner cylinder at velocity $\bar{\Omega}_1 > \Omega_{10}$, thus producing a steady-state vortex. They then discovered that the modulation of the outer cylinder around zero mean could stabilize the flow and return it to Couette azimuthal motion, making the vortices disappear. The interest in this problem arises from the fact that here the modulation increases the mean critical Reynolds number, whereas in the situation described by (1.2) the modulation is destabilizing; moreover the change in critical

Reynolds number is much larger than in the more standard (1.2) case, so that it is easier to detect experimentally. In §4 we present the results of our implementation of Floquet theory and compare them with this experiment.

We have also considered the flow that develops once the critical velocity is exceeded. This is done in §4, where we present some results obtained by means of the initial-value code and compare them with the experiments. Finally §5 contains a discussion.

2. The equations of motion

The Navier–Stokes equations for axisymmetric incompressible flow are

$$\frac{\partial u_\phi}{\partial t} = -\frac{1}{r} \frac{\partial(\psi, u_\phi)}{\partial(r, z)} + \frac{u_\phi}{r^2} \frac{\partial\psi}{\partial z} + \nu \left\{ \frac{1}{r} \frac{\partial}{\partial r} r \frac{\partial}{\partial r} u_\phi + \frac{\partial^2 u_\phi}{\partial z^2} - \frac{u_\phi}{r^2} \right\}, \quad (2.1)$$

$$\frac{\partial Z}{\partial t} = \frac{2u_\phi}{r^2} \frac{\partial u_\phi}{\partial z} - \frac{1}{r} \frac{\partial(\psi, Z)}{\partial(r, z)} + \nu \left\{ \frac{1}{r} \frac{\partial}{\partial r} r \frac{\partial}{\partial r} r^2 Z + \frac{\partial^2 Z}{\partial z^2} \right\}, \quad (2.2)$$

where u_r , u_ϕ and u_z are the components of the velocity in cylindrical coordinates, ψ is the stream function

$$u_r = -\frac{1}{r} \frac{\partial\psi}{\partial z}, \quad (2.3)$$

$$u_z = \frac{1}{r} \frac{\partial\psi}{\partial r}, \quad (2.4)$$

and Z is $1/r$ times the tangential component of the vorticity, so

$$Z = -\frac{1}{r^2} \frac{\partial^2 \psi}{\partial z^2} - \frac{1}{r} \frac{\partial}{\partial r} r \frac{\partial\psi}{\partial r}. \quad (2.5)$$

The nonlinear terms of the form $\partial(f, g)/\partial(r, z)$ are defined as

$$\frac{\partial(f, g)}{\partial(r, z)} = \frac{\partial f \partial g}{\partial r \partial z} - \frac{\partial f \partial g}{\partial z \partial r}. \quad (2.6)$$

The boundary conditions at the lateral walls are

$$u_r = u_z = 0 \quad \text{at} \quad r = R_1, \quad r = R_2, \quad (2.7)$$

$$u_\phi(r = R_1) = \Omega_1 R_1, \quad u_\phi(r = R_2) = \Omega_2 R_2. \quad (2.8)$$

In the case in which both Ω_1 and Ω_2 are constant we know that at small velocity the solution is the azimuthal Couette flow $\mathbf{u} = (0, u_{c0}, 0)$ where

$$u_{c0}(r) = Ar + B/r, \quad (2.9)$$

and A and B are determined by the boundary conditions

$$A = (R_2^2 \Omega_2 - R_1^2 \Omega_1)/(R_2^2 - R_1^2), \quad B = R_1^2 R_2^2 (\Omega_1 - \Omega_2)/(R_2^2 - R_1^2). \quad (2.10)$$

More generally we consider the case in which Ω_1 and Ω_2 are assigned functions of time given by (1.1). Then all the quantities u_ϕ , Z and ψ are functions of time too. It is convenient to replace the azimuthal velocity u_ϕ by

$$u_\phi(r, t) = u_{c0}(r, t) + v(r, t), \quad (2.11)$$

where $u_{c0}(r, t) = A(t)r + B(t)/r$ is the instantaneous Couette flow which at each time

takes care of the boundary conditions (2.7) and (2.8). The boundary conditions for v are simply

$$v(r = R_1, t) = v(r = R_2, t) = 0. \tag{2.12}$$

The stream function satisfies

$$\psi(r = R_1, t) = \psi(r = R_2, t) = \frac{\partial \psi}{\partial r}(r = R_1, t) = \frac{\partial \psi}{\partial r}(r = R_2, t) = 0. \tag{2.13}$$

We can introduce the dimensionless variables $t \rightarrow tv/d^2$, $r \rightarrow x = (r - R_1)/d$, $z \rightarrow \zeta = z/d$, and fields $v \rightarrow vd/\nu$, $Z \rightarrow ZR_2 d^2/\nu$ and $\psi \rightarrow \psi/\nu R_2$. The Reynolds numbers are defined as

$$Re_1 = \Omega_1 R_1 d/\nu, \quad Re_2 = \Omega_2 R_2 d/\nu \tag{2.14}$$

and the assigned drives of the inner and the outer cylinders can be written as

$$Re_1(t) = \overline{Re}_1\{1 + \epsilon_1 \sin(\omega_1 t)\}, \quad Re_2(t) = \overline{Re}_2\{1 + \epsilon_2 \sin(\omega_2 t)\}. \tag{2.15}$$

Here ω_1 and ω_2 are the dimensionless frequencies of modulation; we also use the parameters γ_1 and γ_2 defined by $\omega_1 = 2\gamma_1^2$ and $\omega_2 = 2\gamma_2^2$.

We define the critical Reynolds number in the modulated case as \overline{Re}_{1c} , and the critical Reynolds number in the steady case as Re_{10} .

To study the modulated Taylor–Couette flow we have developed an initial-value code which solves (2.1), (2.2), (2.5), (2.11), made dimensionless, subjected to the drive (2.15) and the boundary conditions

$$v = \psi = \partial\psi/\partial x = 0 \quad \text{at} \quad x = 0, \quad x = 1. \tag{2.16}$$

A detailed description of this numerical work, together with the tests it was subjected to and its properties of stability and convergence, will be published in another paper. Here it suffices to say that the code is based on a spectral method (Marcus 1984). We assume that the cylinders are infinitely long giving spatial periodicity in the axial direction. The axial dimensionless wavenumber is $\alpha = 2\pi/\lambda$, where λ is the wavelength of the vortex cell pair in units of the gap width d . The unknown functions v , Z and ψ are expanded over a double truncated series of Fourier functions axially and of modified Chebyshev polynomials T_n^* radially:

$$\left. \begin{aligned} \psi(x, \zeta, t) &= \sum_{m=1}^{m=M} \sum_{n=1}^{n=N+2} \psi_{mn}(t) \sin(m\alpha\zeta) T_{n-1}^*(x), \\ v(x, \zeta, t) &= \sum_{m=1}^{m=M+1} \sum_{n=1}^{n=N} v_{mn}(t) \cos((m-1)\alpha\zeta) T_{n-1}^*(x), \\ Z(x, \zeta, t) &= \sum_{m=1}^{m=M} \sum_{n=1}^{n=N} Z_{mn}(t) \sin(m\alpha\zeta) T_{n-1}^*(x). \end{aligned} \right\} \tag{2.17}$$

At each time the state of the flow is represented by a vector containing all the coefficients of these truncated series of ψ , v and Z . The integration in time is done by means of a Crank–Nicholson implicit method for the linear terms in (2.1) and (2.2); an Adams–Bashforth method is used for the nonlinear terms. The algorithm has the form

$$PX^{n+1} = QX^n + \frac{1}{2}\Delta t(3Y^n - Y^{n-1}) + G^n,$$

where X^n is the vector X formed by running together the dependent variables ψ_{mn} , v_{mn} and Z_{mn} at time step $n\Delta t$. Y is a vector which depends nonlinearly on X , and G^n is a known vector at time $n\Delta t$. The truncation parameters M and N depend on the

Reynolds number, larger Re requiring larger M and N (Jones 1985); typically $N = 15$, $M = 6$ and the number of time steps per cycle $N_T = 800$ were used, although different values have been taken in different regions of the parameter space. The actual values of M , N , and N_T used for each case are given in the figure captions. We have also developed a program to study the linear stability of the steady Couette flow: the eigenfunctions produced by this program can then be used as initial conditions of arbitrary amplitude for the initial-value code. Otherwise the starting condition can be provided by an initial guess or by making use of a pre-existing state of the flow.

As we have mentioned in the previous section, there is a discrepancy in the literature about the onset of modulated vortices. The numerical work of Carmi & Tustaniwskyj (1981) predicted large negative threshold shifts in disagreement with other theories. To settle this discrepancy we have developed our own implementation of Floquet theory, which will be described in the other paper on numerical methods. Here we simply mention that the Floquet theory is essentially a linear stability theory for an unperturbed state which is periodic in time: a number of orthonormal perturbations of the initial oscillating state are integrated over a cycle by a linearized version of the initial-value code which we have mentioned before. The eigenvalues of the linear mapping from the initial state into the final state determine the stability.

3. The amplitude equation and the effect of imperfections

The amplitude equation for modulated Taylor–Couette flow has been derived by Hall (1975, 1983). The amplitude of the axially periodic Fourier mode obeys a differential equation of the form

$$\frac{dA}{dt} = \{\mu + \epsilon \sin(\omega t)\} A - A^3, \quad (3.1)$$

provided we are sufficiently close to critical Reynolds number. Here t and ω are the time and frequency, suitably scaled in the derivation. μ is proportional to $\overline{Re}_1 - \overline{Re}_{1c}$, where \overline{Re}_{1c} is the critical Reynolds number for the modulated flow. As we see later, the critical Reynolds number is dependent on ϵ and ω , but only rather weakly: determining this dependence has been the main object of most of the experiments and theory mentioned in §1. The main object of the analysis of this section is to explain why many of the experiments have failed to reveal a coherent picture of the dependence of \overline{Re}_{1c} on ϵ and ω , and why they are often in disagreement with the theoretical predictions of Hall (1975, 1983). We believe the reason for this disagreement is not that Hall's analysis is in error; indeed, as we shall show later, our numerical results confirm his analysis. Our view is that many of the onset experiments that have been performed are extremely sensitive to noise that makes the bifurcation imperfect: we can model this noise by adding an additional term to the amplitude equation (3.1), so that it becomes

$$\frac{dA}{dt} = \{\mu + \epsilon \sin(\omega t)\} A - A^3 + c, \quad (3.2)$$

where c is a small constant. Such a term was discussed by Schaeffer (1980) and Hall (1983) in the unmodulated Taylor–Couette problem, and has also been considered in the Rayleigh–Bénard problem as summarized in §1. A detailed derivation and a discussion of this equation has recently been discussed by Lettis (1986).

There are a number of physical effects which can give rise to imperfections, end

effects being the most frequently discussed (e.g. Schaeffer 1980; Benjamin 1978*a, b*). However, many of the experiments we are discussing here were performed in long-aspect-ratio apparatus: for example, in Ahlers' (1988, private communication) experiment, the aspect ratio $\Gamma = h/d$, where h is the length of the cylinders, takes the value $\Gamma = 42.7$. A detailed experimental study of end effects was performed by Walsh & Donnelly (1988*a*) and Walsh (1988). At modulation amplitude $\epsilon_1 = 0.5$ and frequency $\gamma_1 \approx 1.0$ they found the following threshold shifts: at $\eta = 0.718$ and $\Gamma = 30$, $r = -19.9\%$; at $\eta = 0.95$ and $\Gamma = 170$, $r = -16.52\%$; at $\eta = 0.88$ and $\Gamma = 60$, $r = -19.87\%$. Bearing in mind that critical Reynolds numbers are rather insensitive to radius ratio η , we see that the experimental results are also insensitive to Γ over a wide range. In another test, Walsh (1988) found that the axial position of the detector made no significant difference unless it was more than 75% of the distance from the middle of the cylinders to an end. We conclude that end effects are probably not the most important source of imperfections leading to the large change in threshold shifts seen in many experiments. Experimentalists try to eliminate fluctuations in temperature along the cylinders, but nevertheless fluctuations of typical order 10^{-3} K are usually present; these temperature variations give rise to convective motions which lead to non-zero c . Another source of imperfection arises if the cylinders are not absolutely straight: even extremely small variations in the radius of the cylinders of the order of 10^{-2} cm give a variation of the centrifugal acceleration on the sidewalls which leads to a pressure gradient along the sidewalls. The resulting motion renders the bifurcation imperfect. These imperfections can be expected to vary on a long timescale, so that it is reasonable to assume c is a constant: physical effects which would lead to a time-varying c may also be present: numerical investigations of these have been given by Ahlers *et al.* (1985*b*). However, the assumption of constant c allows analytical progress to be made with (3.2).

Before we can attack (3.2), we must first make a few remarks about the 'perfect' amplitude equation (3.1). We follow Hall's (1975) treatment. The general solution of (3.1) can be written

$$\begin{aligned}
 \frac{1}{A^2} = \frac{1}{A_0^2} \exp \left\{ \frac{2\epsilon}{\omega} [\cos(\omega t) - 1] - 2\mu t \right\} \\
 + 2 \exp \left\{ \frac{2\epsilon}{\omega} \cos(\omega t) - 2\mu t \right\} \int_0^t \exp \left\{ 2\mu x - \frac{2\epsilon}{\omega} \cos(\omega x) \right\} dx, \quad (3.3)
 \end{aligned}$$

where A_0 is the initial value of A . If $\mu < 0$ the first term grows exponentially, so that any initial disturbance tends to zero. If μ is positive but small,

$$A \sim \frac{\mu^{\frac{1}{2}} \exp \{ -\epsilon/\omega \cos(\omega t) \}}{[I_0(2\epsilon/\omega)]^{\frac{1}{2}}} \quad (3.4)$$

as $t \rightarrow \infty$, where I_0 is the modified Bessel function of order zero (note that (3.4) is valid only if $\mu \ll \epsilon/\omega$). We conclude from this that $\mu = 0$ corresponds to the critical Reynolds number, and that the amplitude of the motion grows as $\mu^{\frac{1}{2}}$, following the usual Landau law.

As we move through a period of the modulation cycle, the quantity $\mu + \epsilon \sin(\omega t)$, which is proportional to $\overline{Re}_1(1 + \epsilon_1 \sin(\omega t)) - \overline{Re}_{1c}$ and which we may think of as the instantaneous growth rate, is negative for half the cycle and positive for half the cycle at marginal stability $\mu = 0$. If ϵ/ω is fairly large, then (3.4) predicts that the amplitude takes the form of pulses, the ratio of maximum to minimum amplitude being $\exp(2\epsilon/\omega)$. This behaviour is illustrated in figure 1(*a*): note that in the period

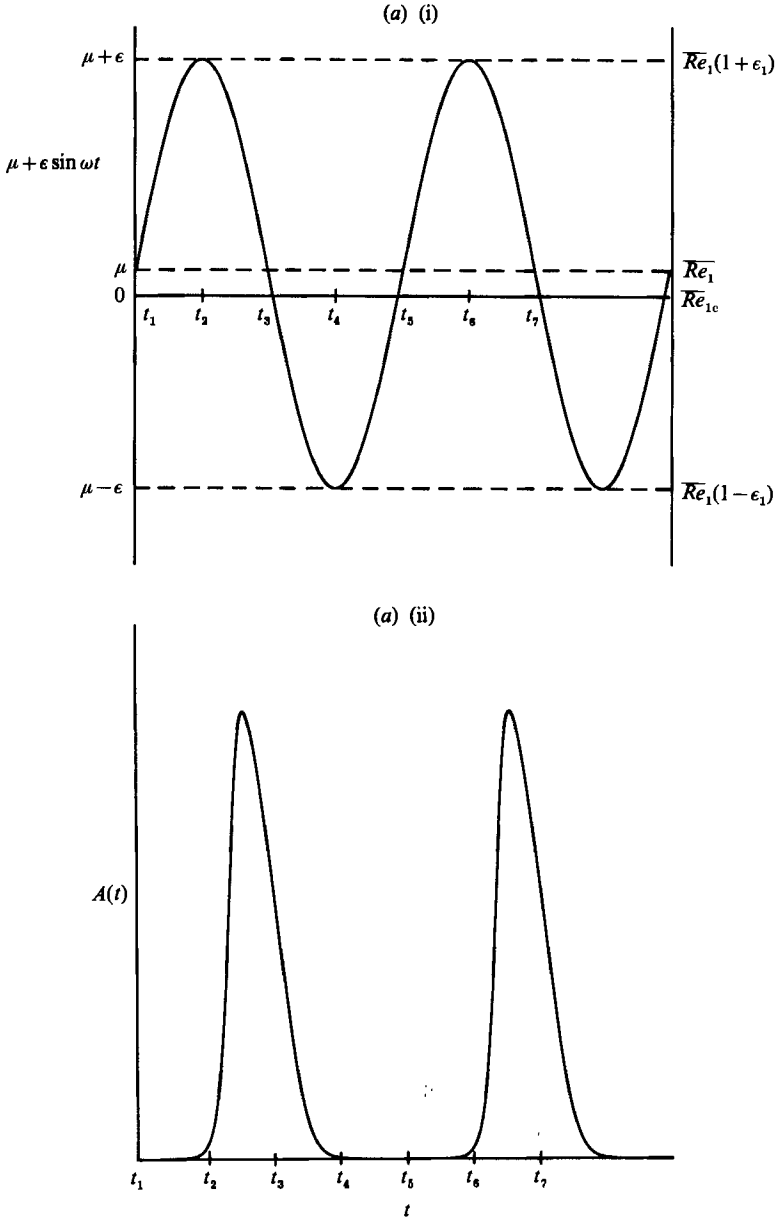


FIGURE 1(a). For caption see facing page.

$t_4 < t < t_6$ the amplitude becomes exponentially small. In practice this is unrealistic, because the weak imperfections mentioned above always drive low-amplitude motions. Furthermore, the effects of the imperfections are not limited to the region $t_4 < t < t_6$ but significantly alter the behaviour at large amplitude in the $t_2 < t < t_4$ range. This idea, and its consequences, have been explored in the context of Bénard convection by Finucane & Kelly (1976). They remarked that even if a particular small disturbance achieves no net growth over a cycle, it is still possible for it to have grown to observable size during the supercritical part of the cycle and then decayed to zero. So the natural occurrence of many disturbances will give rise to observable

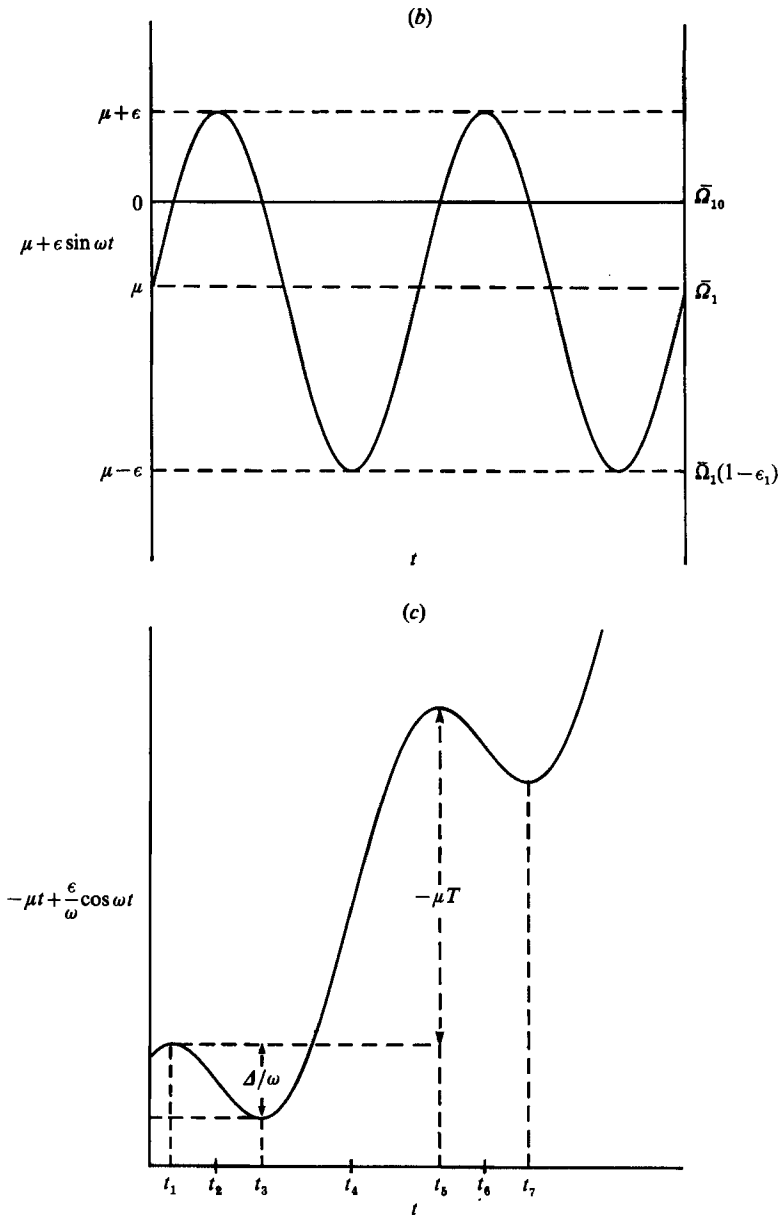


FIGURE 1. (a) (i) Plot of $\mu + \epsilon \sin(\omega t)$ vs. t for $\mu = 0.4$, $\epsilon = 4$ and $\omega = 0.7$. (ii) Sketch of the corresponding amplitude $A(t)$ from (3.1). (b) Plot of $\mu + \epsilon \sin(\omega t)$ vs. t for $\mu = -1$, $\epsilon = 2$ and $\omega = 1$. (c) Plot of $-\mu t + (\epsilon/\omega) \cos(\omega t)$ vs. t for the same μ , ϵ and ω as (b).

motion over part of each cycle. We are therefore led to consider (3.2) especially in the limit when c and ω are small.

A further motivation for studying this problem comes from the experiments. Both Donnelly (1964) and Thompson (1969) reported that at low frequency vortices occur if the maximum Reynolds number $\overline{Re}_1(1 + \epsilon_1)$ during a cycle exceeds the critical Reynolds number Re_{10} for the onset of steady vortices. This remark was also made by Carmi & Tustaniwskyj (1981). On simple physical grounds this seems quite

reasonable, because at low frequency when we are near $t = t_2$ we have a long period when the Reynolds number is above Re_{10} and we would expect to see vortices as we do in the steady problem. Indeed such vortices are observed in experiments and are called 'transient vortices': the name derives from the fact that they are only seen at the top of the cycle, not because they disappear as $t \rightarrow \infty$. Although this behaviour seems reasonable, we should emphasize that it is not what is predicted by the perfect bifurcation theory. This predicts that the critical Reynolds number in the modulated case, \overline{Re}_{1c} is slightly below that for the steady problem Re_{10} , by an amount of order ϵ^2 ; this change in critical Reynolds number is usually much less than $\epsilon_1 \overline{Re}_1$, the amplitude variation of the instantaneous Reynolds number. The transient vortices are therefore being observed in a regime in which \overline{Re}_1 is well below both \overline{Re}_{1c} and Re_{10} ; the typical situation is sketched in figure 1(b). This corresponds to a regime in which $\mu < 0 < \mu + \epsilon$ in (3.1), and as we have seen perfect bifurcation theory predicts that all disturbances decay to zero, in contradiction to the fact that the 'transient' vortices, despite their name, persist as $t \rightarrow \infty$.

We believe that the resolution of this apparent paradox lies in the effect of imperfections in the apparatus. These provide the initial perturbation from which the 'transient' vortices can grow. The reason why there are not transient vortices in the perfect bifurcation theory case when $\mu < 0 < \mu + \epsilon$, even at low frequency, is that the long phase of exponential growth is followed by an even longer phase of exponential decay. This drives the amplitude down to extremely small values which are not physically meaningful. At low frequencies, therefore, we must replace (3.1) by (3.2) which provides a more realistic model. As we see below, the criterion for c to be significant at low frequency is that c should be of order $K^{-1}\omega^{\frac{1}{2}}\exp(-A/\omega)$ or larger, where K and A are numbers of order unity. Because of the exponential factor, the frequency does not have to be very low for even a very small c to achieve this magnitude, and the evidence suggests that in many of the experiments c has been comparable with $K^{-1}\omega^{\frac{1}{2}}\exp(-A/\omega)$.

It is quite instructive (and very straightforward) to integrate (3.1) numerically with $\mu < 0$ and ω small, using a high-accuracy integration routine and double precision, so that machine accuracy is around 10^{-13} . Parameter values of $\mu = -1$, $\epsilon = 2$ and $\omega = 0.1$ are suitable. Despite the fact that we have shown that the analytic solution decays to zero, the numerical solution does not. During the decay phase it drops to around 10^{-12} , at which point rounding errors prevent it from falling even lower; during the next growth phase the solution gets back to an $O(1)$ value before dropping down again. In this numerical experiment the imperfection is provided by rounding error and is of course minute compared with the imperfections in any physical apparatus: nevertheless, these tiny imperfections are sufficient to completely change the $O(1)$ behaviour of the system at low frequency.

We now investigate the asymptotic behaviour of (3.2) in the limit in which ω and c are small. There are a number of different regimes. If $\mu + \epsilon < 0$ no amplification occurs and disturbances remain small. If $\mu - \epsilon > 0$, the instantaneous growth rate is always positive and the imperfection c will not affect the solution significantly unless it is $O(1)$. The case of interest is when

$$\mu - \epsilon < 0 \quad \text{and} \quad \mu + \epsilon > 0; \quad \omega \text{ and } c \text{ are small,} \quad \text{and } \mu, \epsilon \text{ are } O(1). \quad (3.5)$$

In general the periodic solution of (3.2) we are seeking is composed of two regions which must be asymptotically matched. In the neighbourhood of t_3 (see figure 1b), the solution has undergone the exponential growth phase, and in general A will have

reached an $O(1)$ value where it is governed by (3.1), c being then negligible. The solution (3.3) is then applicable and we can write

$$\frac{1}{A^2} = \exp\left\{\frac{2\epsilon}{\omega} \cos(\omega t) - 2\mu t\right\} \left[K_1 \exp\left\{2\mu t_3 - \frac{2\epsilon}{\omega} \cos(\omega t_3)\right\} + \int_{t_1}^t 2 \exp\left\{2\mu x - \frac{2\epsilon}{\omega} \cos(\omega x)\right\} dx \right], \quad (3.6)$$

where K_1 is a constant to be determined by matching.

After a full cycle of length $T = 2\pi/\omega$, in the neighbourhood of t_7 , the solution has to repeat, so it has the form

$$\frac{1}{A^2} = \exp\left\{\frac{2\epsilon}{\omega} \cos(\omega t) - 2\mu t\right\} \left[K_1 \exp\left\{2\mu(t_3 + T) - \frac{2\epsilon}{\omega} \cos(\omega t_3)\right\} + \int_{t_5}^t 2 \exp\left\{2\mu x - \frac{2\epsilon}{\omega} \cos(\omega x)\right\} dx \right]. \quad (3.7)$$

Between these two regions where A is $O(1)$ there is a region where A is small, A^3 is negligible and c is important. In the neighbourhood of t_5 , the governing equation is

$$\frac{dA}{dt} = \{\epsilon \sin(\omega t) + \mu\} A + c, \quad (3.8)$$

with solution

$$A = K_2 \exp\left\{\mu t - \frac{\epsilon}{\omega} \cos(\omega t)\right\} + c \exp\left\{\mu t - \frac{\epsilon}{\omega} \cos(\omega t)\right\} \int_{t_3}^t \exp\left\{-\mu x + \frac{\epsilon}{\omega} \cos(\omega x)\right\} dx. \quad (3.9)$$

The quantity inside the exponential in the integral in (3.9) plays a crucial role in understanding the matching procedure, so it sketched in figure 1(c). Provided (3.5) holds, it has successive maxima and minima; the case drawn is for $\mu < 0$: if $\mu > 0$ successive maxima decline rather than rise. We now determine the constants K_1 and K_2 by matching (3.9) to (3.6) and (3.7). The quantity inside the integral in (3.6) is the exponential of -2 times the quantity plotted in figure 1(c). Once t goes past t_3 into the exponential decline phase which follows t_3 , this integral is dominated by the contribution near t_3 . The method of steepest descent can be used to evaluate the integral:

$$\int_{t_1}^t 2 \exp\left\{2\mu x - \frac{2\epsilon}{\omega} \cos(\omega x)\right\} dx = \int_{t_1-t_3}^{t-t_3} 2 \exp\left\{2\mu(t_3 + \tau) - \frac{2\epsilon}{\omega} \left[\cos(\omega t_3) \cos(\omega \tau) - \sin(\omega t_3) \sin(\omega \tau) \right]\right\} d\tau.$$

Expanding in powers of $\omega \tau$ (ω is small), and using $\mu + \epsilon \sin(\omega t_3) = 0$,

$$\begin{aligned} \int_{t_1}^t 2 \exp\left\{2\mu x - \frac{2\epsilon}{\omega} \cos(\omega x)\right\} dx &\approx \exp\left\{2\mu t_3 - \frac{2\epsilon}{\omega} \cos(\omega t_3)\right\} \int_{-\infty}^{\infty} 2 \exp\left\{\epsilon \omega \tau^2 \cos(\omega t_3)\right\} d\tau, \\ &\approx \exp\left\{2\mu t_3 - \frac{2\epsilon}{\omega} \cos(\omega t_3)\right\} \left[\frac{4\pi}{-\epsilon \omega \cos(\omega t_3)} \right]^{\frac{1}{2}}. \end{aligned}$$

So, from (3.6), the behaviour in the exponential decline phase following t_3 is

$$A \approx \exp\left\{\mu t - \frac{\epsilon}{\omega} \cos(\omega t)\right\} \left[K_1 + \left[\frac{4\pi}{-\epsilon\omega \cos(\omega t_3)} \right]^{\frac{1}{2}} \right]^{-\frac{1}{2}} \exp\left\{-\mu t_3 + \frac{\epsilon}{\omega} \cos(\omega t_3)\right\}. \quad (3.10)$$

This has to agree with the behaviour of (3.9) in this region. Now in this region the c -term is growing from a small value; it is then K_2 that matches the behaviour (3.10). So

$$K_2 = \left[K_1 + \left[\frac{4\pi}{-\epsilon\omega \cos(\omega t_3)} \right]^{\frac{1}{2}} \right]^{-\frac{1}{2}} \exp\left\{-\mu t_3 + \frac{\epsilon}{\omega} \cos(\omega t_3)\right\}. \quad (3.11)$$

As t increases past t_3 , the c -term in (3.9) increases, but the quantity inside the integral attains a maximum at $t = t_5$ and so the regime $t > t_5$ corresponds to exponential growth. We again use steepest descent to evaluate the integral asymptotically just as we did to evaluate (3.10). We obtain

$$A \approx \exp\left\{\mu t - \frac{\epsilon}{\omega} \cos(\omega t)\right\} \left[K_2 + c \exp\left\{-\mu t_5 + \frac{\epsilon}{\omega} \cos(\omega t_5)\right\} \left[\frac{2\pi}{\epsilon\omega \cos(\omega t_5)} \right]^{\frac{1}{2}} \right]$$

here: also from (3.7) in the regime just beyond t_5 ,

$$A \approx \exp\left\{\mu t - \frac{\epsilon}{\omega} \cos(\omega t)\right\} K_1^{-\frac{1}{2}} \exp\left\{-\mu(t_3 + T) + \frac{\epsilon}{\omega} \cos(\omega t_3)\right\},$$

and matching gives

$$K_2 + c \exp\left\{-\mu t_5 + \frac{\epsilon}{\omega} \cos(\omega t_5)\right\} \left[\frac{2\pi}{\epsilon\omega \cos(\omega t_5)} \right]^{\frac{1}{2}} = K_1^{-\frac{1}{2}} \exp\left\{-\mu(t_3 + T) + \frac{\epsilon}{\omega} \cos(\omega t_3)\right\}. \quad (3.12)$$

Eliminating K_2 from (3.11) and (3.12) and defining

$$K = \left[\frac{2\pi}{\epsilon \cos(\omega t_1)} \right]^{\frac{1}{2}} = \left[\frac{2\pi}{(\epsilon^2 - \mu^2)^{\frac{1}{2}}} \right]^{\frac{1}{2}}, \quad (3.13)$$

$$A_m = cK\omega^{-\frac{1}{2}} \exp\left\{\mu(t_3 - t_1) - \frac{\epsilon}{\omega} [\cos(\omega t_3) - \cos(\omega t_1)]\right\} = cK\omega^{-\frac{1}{2}} \exp(A/\omega), \quad (3.14)$$

where

$$A/\omega = [2\mu\{\frac{1}{2}\pi + \sin^{-1}(\mu/\epsilon)\} + 2(\epsilon^2 - \mu^2)^{\frac{1}{2}}]/\omega$$

is the distance marked in figure 1(c), we obtain

$$A_m + \frac{\exp(\mu T)}{[K_1 + (2K^2/\omega)^{\frac{1}{2}}]^{\frac{1}{2}}} - K_1^{-\frac{1}{2}} = 0, \quad (3.15)$$

which is the matching equation. Note that K_1 , K , A_m and T are all positive quantities, and that A_m is the term proportional to c , the imperfection. We now break the discussion down into various cases:

(i) $\mu < 0$, i.e. the Reynolds number is below the critical value for a perfect bifurcation. No solution is possible unless A_m is significant, i.e. the imperfection is significant. The second term is negligible compared to the third, so

$$K_1 \approx \frac{1}{A_m^2} \quad (3.16)$$

and (3.6) becomes

$$\frac{1}{A^2} = \exp\left\{\frac{2\epsilon}{\omega} \cos(\omega t) - 2\mu t\right\} \left[\frac{1}{A_m^2} \exp\left\{2\mu t_3 - \frac{2\epsilon}{\omega} \cos(\omega t_3)\right\} + \int_{t_1}^t 2 \exp\left\{2\mu x - \frac{2\epsilon}{\omega} \cos(\omega x)\right\} dx \right]. \quad (3.17)$$

Provided $t_1 < t < t_3$ we may approximate the integral, since from figure 1(c) it is dominated by the behaviour at t (there is no internal maximum in this case, the integrand increases monotonically). We have

$$\begin{aligned} & \int_{t_1}^t 2 \exp\left\{2\mu x - \frac{2\epsilon}{\omega} \cos(\omega x)\right\} dx \\ & \approx 2 \int_{t_1-t}^0 2 \exp\left\{2\mu(\tau+t) - \frac{2\epsilon}{\omega} \cos(\omega\tau) \cos(\omega t) + \frac{2\epsilon}{\omega} \sin(\omega\tau) \sin(\omega t)\right\} d\tau \\ & \approx 2 \exp\left\{2\mu t - \frac{2\epsilon}{\omega} \cos(\omega t)\right\} \int_0^\infty \exp\{-2\mu\tau - 2c\tau \sin(\omega t)\} d\tau \\ & = \frac{\exp\{2\mu t - 2\epsilon/\omega \cos(\omega t)\}}{\mu + \epsilon \sin(\omega t)}. \end{aligned}$$

So (3.17) becomes

$$\frac{1}{A^2} = \frac{1}{A_m^2} \exp\left\{2\mu(t_3-t) + \frac{2\epsilon}{\omega} \left[\cos(\omega t) - \cos(\omega t_3)\right]\right\} + \frac{1}{\mu + \epsilon \sin(\omega t)}, \quad t_1 < t < t_3. \quad (3.18)$$

The two terms on the right-hand side of (3.18) can be easily interpreted: if the second term is dominant $A \approx (\mu + \epsilon \sin(\omega t))^{\frac{1}{2}}$, which is the ‘quasi-static’ local equilibration value, i.e. the value A has if dA/dt is neglected in (3.1). The first term contains the noise and determines how long it takes before local equilibration is achieved: if c is very small so is A_m , and the longer it takes before local equilibration is achieved; indeed, if

$$A_m \ll 1 \quad (3.19)$$

local equilibration is never achieved, and the solution never gets to $A \sim O(1)$. A_m then dominates the maximum value that A achieves. Because of the $\exp(\Delta/\omega)$ factor in (3.14), the value of c has to be extremely small at low frequency for A not to reach an $O(1)$ value. This enables us to give a criterion for whether c is large enough for $O(1)$ transient vortices to occur: if

$$c \ll c_- = \omega^{\frac{1}{2}} \exp(-\Delta/\omega)/K \quad (3.20)$$

(c_- because this is the $\mu < 0$ criterion), then the imperfection is too small for $O(1)$ vortices to occur, and in experiments the effects of the imperfection will not be observed. If $c \approx c_-$ or larger, $O(1)$ transient vortices will be seen.

(ii) $\mu > 0$, i.e. the Reynolds number is above the critical value of a perfect bifurcation. $\exp(\mu T)$ is now large so K_1 is small in (3.15), so K_1 is small compared to $(2K^2/\omega)^{\frac{1}{2}}$. Therefore

$$K_1 \approx \left[A_m + \frac{\exp(\mu T)}{(2K^2/\omega)^{\frac{1}{2}}} \right]^{-2}. \quad (3.21)$$

The criterion for imperfection to be negligible in this $\mu > 0$ case is $A_m \ll \exp(\mu T)/(2K^2/\omega)^{\frac{1}{2}}$, which is equivalent to

$$c \ll c_+ = \frac{\omega^{\frac{3}{2}}}{2^{\frac{1}{2}}K^{\frac{3}{2}}}\exp(\mu T - \Delta/\omega). \quad (3.22)$$

If this criterion is violated, A_m is significant and its effect is to reduce K_1 . Since, by a similar argument to that used to obtain (3.18),

$$\frac{1}{A^2} = K_1 \exp\left\{2\mu(t_3 - t) + \frac{2\epsilon}{\omega}[\cos(\omega t) - \cos(\omega t_3)]\right\} + \frac{1}{\mu + \epsilon \sin(\omega t)}, \quad t_1 < t < t_3, \quad (3.23)$$

the effect of adding the noise is to make A achieve 'local equilibration' earlier in the cycle. Numerical integration of (3.2) confirms this effect: it is discussed in relation to the experiments in §4.

We summarize the most important findings of the analysis:

(i) If $\mu < 0$ and $c \ll c_-$ then the amplitude A never reaches $O(1)$, but only achieves a maximum of $cK\omega^{-\frac{1}{2}}\exp(\Delta/\omega)$.

(ii) If $\mu < 0$ and $c \approx c_-$ then A reaches local equilibration during the cycle (transient vortices). The larger c , the earlier local equilibration is reached; if c is relatively small, local equilibration is only achieved near t_3 , but if c is much larger than c_- local equilibration holds almost from t_1 to t_3 .

(iii) If $\mu > 0$ then if $c \ll c_+$ noise is unimportant; if c is comparable with c_+ the first effect of the noise is to make the growth phase of A occur earlier in the cycle.

4. The results and comparison with experiments

We first look at the case in which the outer cylinder is fixed and the inner cylinder is modulated around non-zero mean,

$$\left. \begin{aligned} Re_1(t) &= \overline{Re}_1(1 + \epsilon_1 \sin(\omega_1 t)), \\ Re_2(t) &= 0. \end{aligned} \right\} \quad (4.1)$$

The first question that we consider is the Reynolds number \overline{Re}_{1c} for the onset of vortices in the modulated case at given ϵ_1 and ω_1 . If we define Re_{10} as the Reynolds number for the onset of vortices in the steady-state situation, we want to know whether the threshold shift $r = (\overline{Re}_{1c} - Re_{10})/Re_{10}$ is big and negative, i.e. the modulation strongly destabilizes the flow, as claimed by Carmi & Tustaniwskyj (1981), or rather r is small and negative, i.e. the modulation weakly destabilizes the flow, as claimed by Hall (1975).

In figure 2 we compare our numerical calculations of Floquet exponents with those of Carmi & Tustaniwskyj by plotting r as a function of γ_1 at $\epsilon_1 = 0.5$ and $\eta = 0.6925$. One can see that there is disagreement over the order of magnitude: we had to multiply our threshold shifts by 10 to make them visible on the same graph together with the results of Carmi & Tustaniwskyj. For example at their lowest frequency $\gamma_1 = 1$ we find $r = -0.8\%$ against their $r = -30.6\%$. The source of this disagreement must be numerical. At first we suspected that Carmi & Tustaniwskyj used too few Galerkin modes (typically only 3 or 4): we therefore investigated the effect of severe mode truncation on our collocation scheme, by reducing the number of polynomials used. This failed to reproduce their large threshold shifts: the results were consistent with our high-resolution runs until the truncation was reduced to a very small

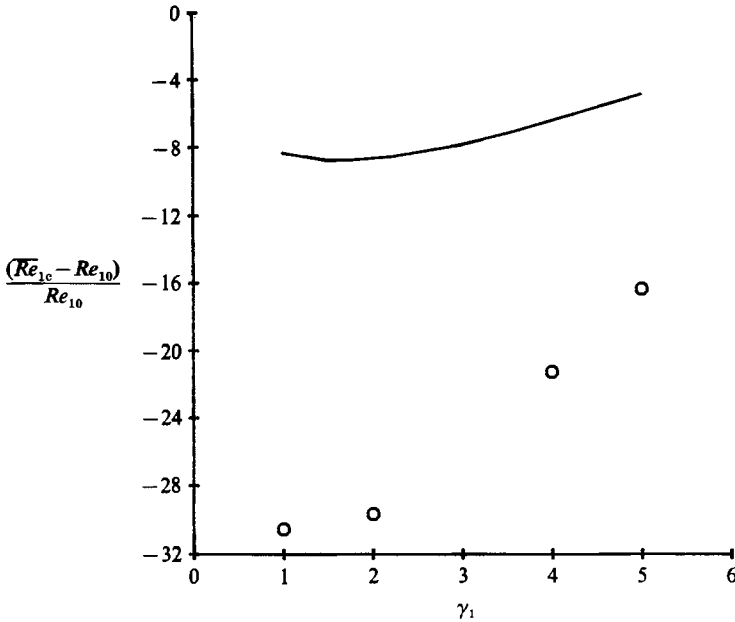


FIGURE 2. Comparison with Carmi & Tustaniwskyj (1981). Plot of threshold shifts $100(\overline{Re}_{1c} - Re_{10})/Re_{10}$ vs. γ_1 at $\eta = 0.6925$ and $\epsilon_1 = 0.5$ with outer cylinder fixed: circles, data of Carmi & Tustaniwskyj; solid line, our results multiplied by 10. We used $\alpha = 3.13$, $N = 15$, $N_T = 800$.

| At $\gamma_1 = 10$ | Steps per cycle | \overline{Re}_{1c} |
|--------------------|-----------------|----------------------|
| | 1000 | 78.63 |
| | 500 | 78.63 |
| | 100 | 78.64 |
| | 60 | 78.67 |
| | 30 | 78.77 |
| At $\gamma_1 = 1$ | 1600 | 78.02 |
| | 800 | 78.06 |
| | 100 | 64.79 |
| | 60 | 42.06 |
| | 30 | 23.90 |

TABLE 1. Critical Reynolds numbers \overline{Re}_{1c} at $\eta = 0.6925$, $\epsilon_1 = 0.5$, $\alpha = 3.13$ as a function of time step. We use $N = 15$ Chebyshev polynomials.

number of polynomials. Finally we discovered what we believe to be the true source of the disagreement: the time step used in the integrations of their Galerkin truncations. After the introduction of the scaled time $\tau = \omega_1 t$, they claimed a four-digit precision for the stability boundary with a time step $\Delta\tau = 2\pi/30$. We therefore examined the effect of varying the time step in our numerical code. Some results are given in table 1, in which we compute a critical Reynolds number at two different frequencies. At high modulation frequency ($\gamma_1 = 10$) the time step is not very critical and the value used by Carmi & Tustaniwskyj gives reasonable results. At low frequency ($\gamma_1 = 1$) the situation is completely different, and even at 100 steps per cycle a substantial reduction in critical Reynolds number is found. In order to eliminate this bogus threshold change over 500 steps per cycle are needed. We

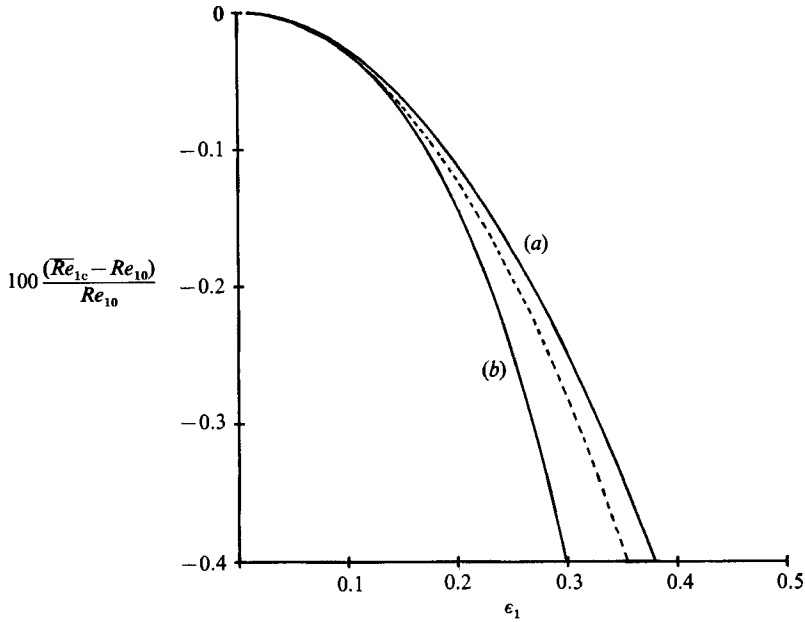


FIGURE 3. Comparison with Hall (1975). Plot of threshold shifts $100(\overline{Re}_{1c} - Re_{10})/Re_{10}$ vs. ϵ_1 at $\eta = 0.999$ and $\omega_1 = 3.49$. The dashed line is our result with $\alpha = 3.1266$, $N = 15$ and $N_T = 800$: curve (a) is Hall's equation (1.3); curve (b) is Hall's equation (1.3) modified by adding the next-order term $-1300 \epsilon_1^4$.

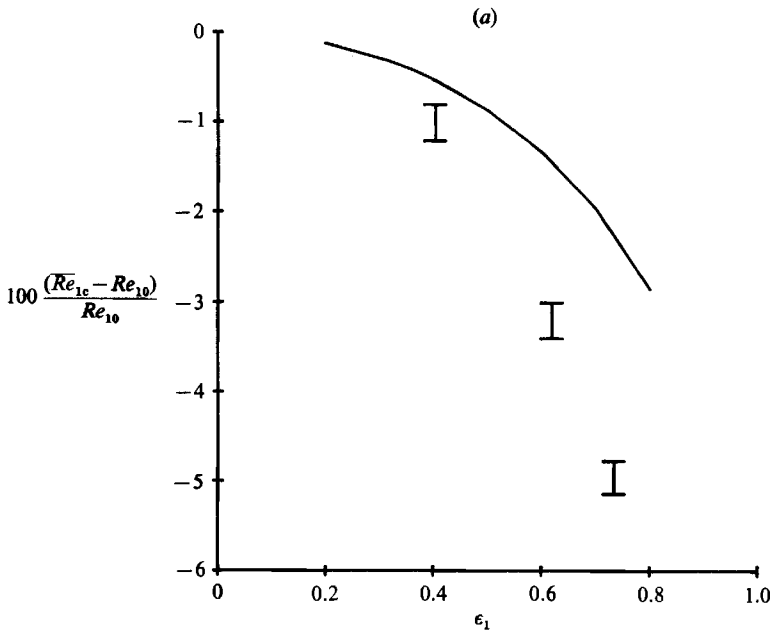


FIGURE 4(a). For caption see facing page.

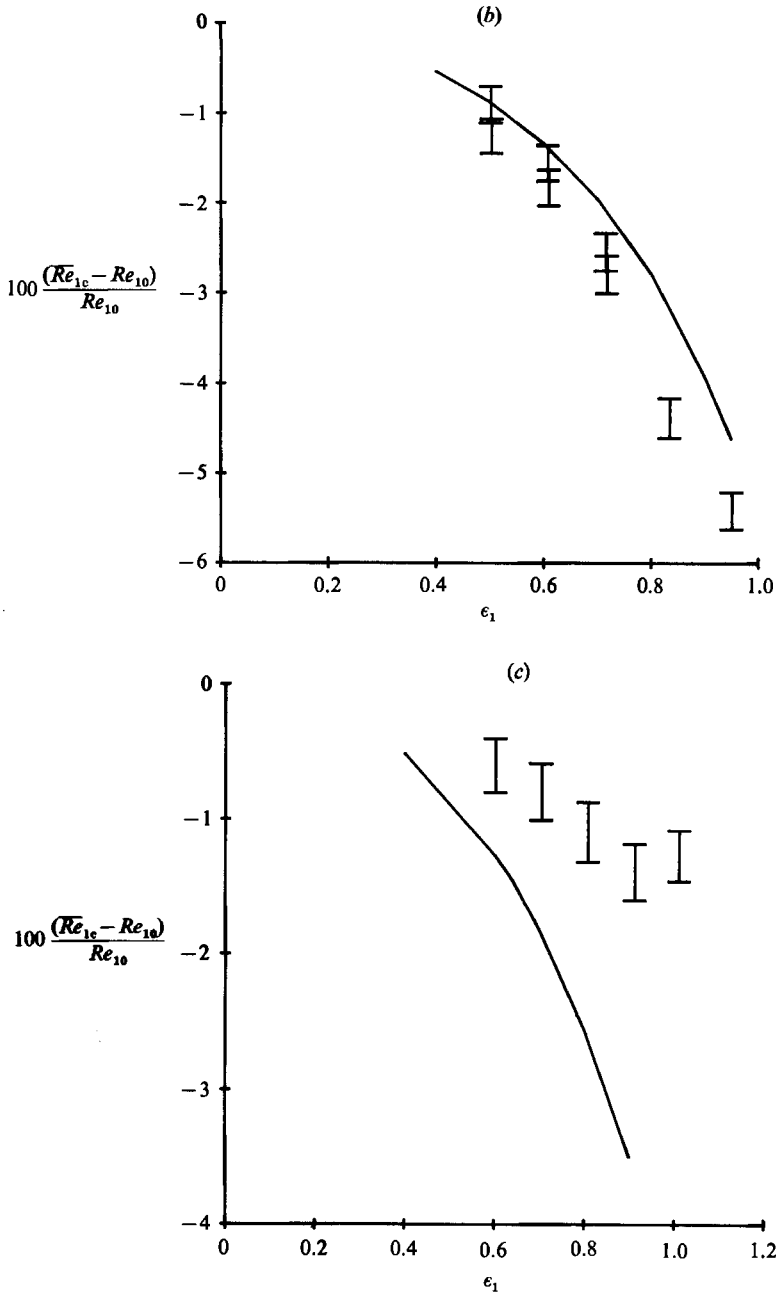


FIGURE 4. Comparison with the experiment of Ahlers (1988, private communication) at $\eta = 0.75$ and (a) $\omega_1 = 4$, (b) $\omega_1 = 6$, (c) $\omega_1 = 8$. Plot of thresholds shifts $100(\overline{Re}_{1c} - Re_{10})/Re_{10}$ vs. ϵ_1 : solid curve, our calculations with $\alpha = 3.13$, $N = 15$, $N_T = 800$; bars, experiment.

therefore conjecture that Carmi & Tustaniwskyj decided on their time step on the basis of tests at fairly high frequency, and were therefore misled by their results at low frequency. Although in principle numerical tests should be performed in *all* parameter regimes in computational work, in practice this is not always feasible. The effect arises because at low frequency the amplitude falls to very low values during

the cycle, as mentioned in the previous section. With too large a time step the numerical solution ‘jumps’ across this part of the cycle too fast, and fails to compute the very small velocities sufficiently accurately. Having too large a time step introduces a numerical imperfection into the system which produces a broadly similar effect to a physical imperfection.

In figure 3 we compare our numerical results with the narrow-gap theory of Hall (1975). The dashed curve gives our computed threshold shifts at $\omega_1 = 3.49$ and $\eta = 0.999$ as a function of ϵ_1 . Hall’s findings are expressed by (1.3), which he presented in his paper over the range $0 < \omega_1 < 6$. To obtain r from (1.3) we transform Hall’s critical Taylor number Ta_c into a Reynolds number at $\eta = 0.999$; Ta_0 is obtained from $Re_{10} = 1302.008$ found by our linear stability program at the same radius ratio: the result is curve (a) in figure 3. In his 1975 paper Hall remarked that the next term in the series (1.3) is $-1300\epsilon_1^4$. We add this term to (1.3) to recompute r and produce the solid curve (b) in figure 3. Our results fall in between the two curves predicted by Hall’s theory.

In the case (4.1) we always found destabilization, in contradiction to the very severely truncated Kuhlmann (1985) model; no sign of the stabilization at high frequency found by the (again severely truncated) Bhattacharjee *et al.* (1986) model emerged from our calculations. We were able to obtain stabilization for some very severe truncations of our expansion, but this behaviour never persisted when more modes were added. We note that the more recent Kuhlmann *et al.* (1988) model with more modes added predicts destabilization. Since the destabilization is such a small effect, it is perhaps not surprising that very severe truncations are not adequate to investigate it.

We conclude therefore that our findings are in disagreement with those of Carmi & Tustaniwskyj but they agree with the prediction of weak destabilization of Hall, which has been recently confirmed also by Kuhlmann *et al.* (1988) by a finite-difference approach. The results of our theory are also in agreement with the experiments of Ahlers performed at finite radius ratio $\eta = 0.75$ with $d = 0.63$ cm. Figures 4(a), 4(b) and 4(c) show our computed threshold shifts and Ahlers’ experimental data at frequencies $\omega_1 = 4, 6$ and 9 respectively. The agreement is reasonable, especially when we consider that the small value of r makes its determination a difficult experiment, and adds to the evidence that the modulation of the inner cylinder produces an $r = O(\epsilon_1^2)$ destabilization.

Having reached this first conclusion we still have to explain why a number of experimental investigations such as those of Thompson (1969) and Walsh & Donnelly (1988a) found a larger $r = O(\epsilon_1)$ destabilization. In §3 we have argued that it is the imperfections of the system that are responsible for this effect and we have developed a theory which makes use of the amplitude equation to take the imperfections into account. To make further quantitative progress we need now to learn how to connect the amplitude equation to the experimental measurements and the numerical calculations.

To do this we have to identify the quantities μ, ϵ, ω, A and c which appear in (3.2). We can set ω to be the usual dimensionless frequency ω_1 defined earlier. At small amplitude in the steady-state case μ is simply the growth rate σ . By using the linear stability program we can compute the growth rate at a particular value of η and α , the axial wavenumber. Since μ is proportional to $(Re_1 - \bar{Re}_{1c})$ near the critical, we need to compute $d\sigma/dRe$ at $\bar{Re}_1 = \bar{Re}_{1c}$. For comparison with experimental data we take $\alpha = 3.13$, close to the first mode to become unstable by steadily rotating linear theory, since there is experimental evidence that the wavenumber does not change

significantly from this value in the modulated case (Ahlers 1988, private communication). As an example, at Ahlers' values $\eta = 0.75$ and $\alpha = 3.13$, $d\sigma/dRe = 0.31$ at $Re_1 = Re_{10} = 85.7766$ was found by our linear stability program, in our dimensionless units. μ will actually be weakly dependent on ω , because the growth rate will not be exactly the same in the oscillatory case as in the steady case, but we ignore this small effect and choose $\mu = (\overline{Re}_1 - \overline{Re}_{1c}) d\sigma/dRe$ with $d\sigma/dRe$ evaluated near Re_{10} . We define ϵ to be consistent with the definition of μ , so we set $\epsilon = (d\sigma/dRe) \overline{Re}_1 \epsilon_1$, where again the derivative is evaluated for the steady case at Re_{10} . Now we have to connect the amplitude A to the value of a velocity component, u_z for example. Let $A = ku_z$. We then use the initial-value code with a steady rotation to evaluate u_z at a desired point for an appropriate value of \overline{Re}_1 . Since in the steady case the amplitude equation gives $A = \mu^{1/2}$ we determine k by setting $k = \mu^{1/2}/u_z$. Since the numerical code gives $u_z \propto (\overline{Re}_1 - \overline{Re}_{1c})^{1/2}$ sufficiently close to critical, the exact value of \overline{Re}_1 at which k is determined is not especially important.

The appropriate value of c is harder to estimate as we can only speculate on the most important sources of imperfection. If we assume that lateral variations of temperature of the order of $\Delta T = 10^{-3}$ K are present on the sidewalls, as estimated by Heinrichs *et al.* (1988), we estimate that

$$\frac{\pi^3 \nu^2 \partial u_z}{d^3 \partial t} \approx g \tilde{\alpha} \Delta T, \quad (4.2)$$

where $\tilde{\alpha}$ is the expansion coefficient and g the acceleration due to gravity; using our dimensionless units for u_z and t

$$\frac{dA}{dt} \approx \frac{g \tilde{\alpha} \Delta T k d^3}{\pi^3 \nu^2} \approx c. \quad (4.3)$$

Taking $\alpha = 0.0002$, $\nu = 0.01 \text{ cm}^2 \text{ s}^{-1}$ for water at 20 °C, and $d = 0.63 \text{ cm}$, $k \approx 0.5$ (see below) we obtain

$$c \approx 8 \Delta T \approx 10^{-2}. \quad (4.4)$$

In practice we believe that c is likely to be less than this for the following reason: in order to be properly represented as a c -term in the amplitude equation the imperfection has to have the same spatial structure as the Taylor vortices. In particular it has to have the same spatial periodicity of $\alpha = 3.13$. In practice it is likely that the dominant axial wavelength of thermal imperfections will be much longer than this, of order the total length of the apparatus. The component of thermal fluctuation with the resonant wavelength is likely to be substantially less, making c correspondingly smaller.

Another source of imperfection is variation of the radius of the cylinders along their length. Heinrichs *et al.* estimate a possible variation $\Delta l \approx 10^{-3} \text{ cm}$. Since a variation in radius gives a fluctuation in the centrifugal acceleration along the length of the cylinders, a pressure gradient along the cylinders is set up:

$$\frac{1}{\rho} \frac{dp}{dz} \approx \frac{\Omega^2 R \Delta l}{d}, \quad (4.5)$$

so

$$\frac{\pi^3 \nu^2 \partial u_z}{d^3 \partial t} \approx \frac{\Omega^2 R \pi \Delta l}{d},$$

which leads to

$$\frac{dA}{dt} \approx \frac{\Omega^2 R k \Delta l d^2}{\pi^2 \nu^2} \approx c. \quad (4.6)$$

Again taking values appropriate to Ahlers' experiment, $\Omega \approx 0.5 \text{ s}^{-1}$, $R \approx 2.5 \text{ cm}$ gives

$$c \approx 120\Delta l \approx 10^{-1}. \quad (4.7)$$

For the same reason as before the effective value of c will be considerably less than this: there is no reason to suppose that variations in radius will have the same axial wavelength as the Taylor vortices.

There are, of course, other possible sources of imperfections such as end effects and the effect of density variations induced by the flow visualization material, often Kalliroscope flakes. The latter problem has been investigated by Dominguez-Lerma, Ahlers & Cannell (1985): they discovered that if the Couette apparatus is mounted vertically, the Taylor-vortex flow has vortex pairs of variable width, due to a non-uniform distribution of Kalliroscope flakes. This effect disappears if the apparatus is mounted horizontally, and Ahlers' (1988, private communication) experiments were performed on a horizontal apparatus. However, it is also found that there is a tendency for Kalliroscope flakes to drift towards the cores of the Taylor vortices. This effect may be particularly important because the density fluctuation has the same spatial periodicity as the vortices themselves.

We can estimate the effective value of c in the data of Walsh & Donnelly (1988*a*) for modulation of the inner cylinder at radius ratio $\eta = 0.88$ and $\epsilon_1 = 0.5$ provided certain assumptions are made. Note that Walsh & Donnelly used Kalliroscope flow visualization and performed their experiments at frequencies as low as $\omega_1 = 0.48$, so we expect their experiment to be more susceptible to the effects of the imperfections than Ahlers' laser-Doppler measurements at $\omega_1 = 4$. In fact Walsh & Donnelly found a large drop in critical Reynolds number at low frequency which we interpret in the following way. The flow was actually below the critical Reynolds number, but the imperfection was amplified in the way described in §3, so the vortices found at low frequency are transient vortices in the same sense described in §3. We assume that the threshold amplitude that the experiment could detect was fixed at $A = 0.2$, which corresponds to the amplitude achieved in a steady-state experiment at a Reynolds number of about 0.1 above critical for this radius ratio (we assume that the axial wavenumber is fixed at 3.13). We define \bar{Re}_{1T} to be the critical value at which the maximum amplitude of the transient vortices is $A = 0.2$. We further assume that the imperfection c is fixed at a value 0.001, which is reasonable in view of the previous estimates (4.4) and (4.7). Since the value of $A = 0.2$ is sufficiently small for us to be in the small-amplitude regime of §3, we can use (3.14) to give an estimate of the maximum amplitude, so we set

$$A_m = 0.2 = 0.001 K \omega^{-\frac{1}{2}} \exp(A/\omega). \quad (4.8)$$

In the experiment $\epsilon_1 = 0.5$, $Re_{10} = 120.5$ and $d\sigma/dRe = 0.22$ at $\bar{Re}_1 = \bar{Re}_{1c} \approx Re_{10}$, so $\epsilon = 13.3$. Then (4.8) becomes a relation between μ and ω which we can connect to a relation between \bar{Re}_{1T} and ω using $\mu = 0.22(\bar{Re}_{1T} - \bar{Re}_{1c})$. In principle \bar{Re}_{1c} should be computed using our Floquet program at different values of ω_1 ; however, since the theoretical threshold shifts are very small on the scale in which we are interested, it is sufficient to approximate $\bar{Re}_{1c} \approx Re_{10}$. The solid curve of figure 5 gives the $\bar{Re}_{1T}-\omega$ relation, and the circles the data of Walsh & Donnelly (1988*a*). The horizontal line is the curve for the onset of instability which we take as $\bar{Re}_{1c} \approx 120$. The broken line is derived by direct numerical integration of the amplitude equation by fitting μ so that $A_m = 0.2$ at a given ω_1 : it overlaps the solid line everywhere but in the region $\bar{Re}_1 \approx \bar{Re}_{1c}$, thus showing that the asymptotic solution (represented by the solid line) is a good approximation. From the fact that the solid (or broken) curve and the

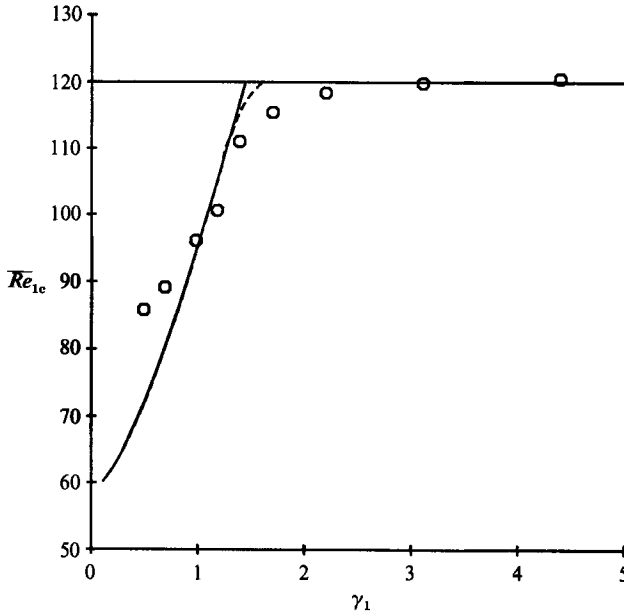


FIGURE 5. Effect of the imperfection in Walsh & Donnelly's (1988*a*) experiment. Plot of the critical \overline{Re}_{1c} vs. γ_1 at $\eta = 0.88$ and $\epsilon_1 = 0.5$: circles, experimental data; solid curve, computation of $c = 0.001$ imperfection by using equation (4.8). Broken curve, the same as the solid line but the amplitude equation was integrated numerically.

circles lie fairly close together, we infer that $c = 0.001$ is a reasonable estimate of the imperfection level. In view of the estimates (4.4) and (4.7), it is rather remarkable that the experimentalists have managed to keep the imperfection to so low a level: however, it is in the nature of the problem that the only effect of reducing the amount of the imperfection would be to shift the shoulder of the solid curve in figure 5 further to the left. Also, because of the exponential dependence on ω , a very large reduction in the imperfection c results in only a modest shift of the shoulder to the left.

It is difficult to incorporate imperfections such as thermal gradients into the initial-value code directly, as the resulting equations are considerably harder to solve. The main effect of such an imperfection will be to generate a source term of potential vorticity Z ($1/r$ times the azimuthal vorticity). This will also be the main effect of an axisymmetric geometrical imperfection of the inner cylinder wall. It is therefore reasonable to model the imperfection by adding a source of potential vorticity to the right-hand side of (2.2). Since we do not know the precise form of the imperfection, we adopt two simple models for the vorticity source.

In the first model we assume that the source of vorticity has the form $\partial Z/\partial t = c \sin \alpha \zeta$, so that only the first Fourier component is excited, and the source is uniform across the gap. In the second model we assume that the vorticity is concentrated near the inner cylinder (to represent, for example, a geometrical distortion), so that the no-slip boundary condition is changed to $\partial \psi/\partial x = -0.5c \Delta t \eta (1 + \eta) \sin \alpha \zeta$. This choice implies that the r -averaged potential vorticity, $\int_{R_1}^{R_2} Z r dr$, is the same in both models if c is the same. Figures 6(a) and 6(b) show that in both cases we can produce a Taylor-vortex flow steadily oscillating at low frequency at Reynolds number $\overline{Re}_1 < \overline{Re}_{10}$ i.e. a 'transient' vortex. Without the source of vorticity, on the contrary, we find the expected result that any initial disturbance decays to zero, since then the

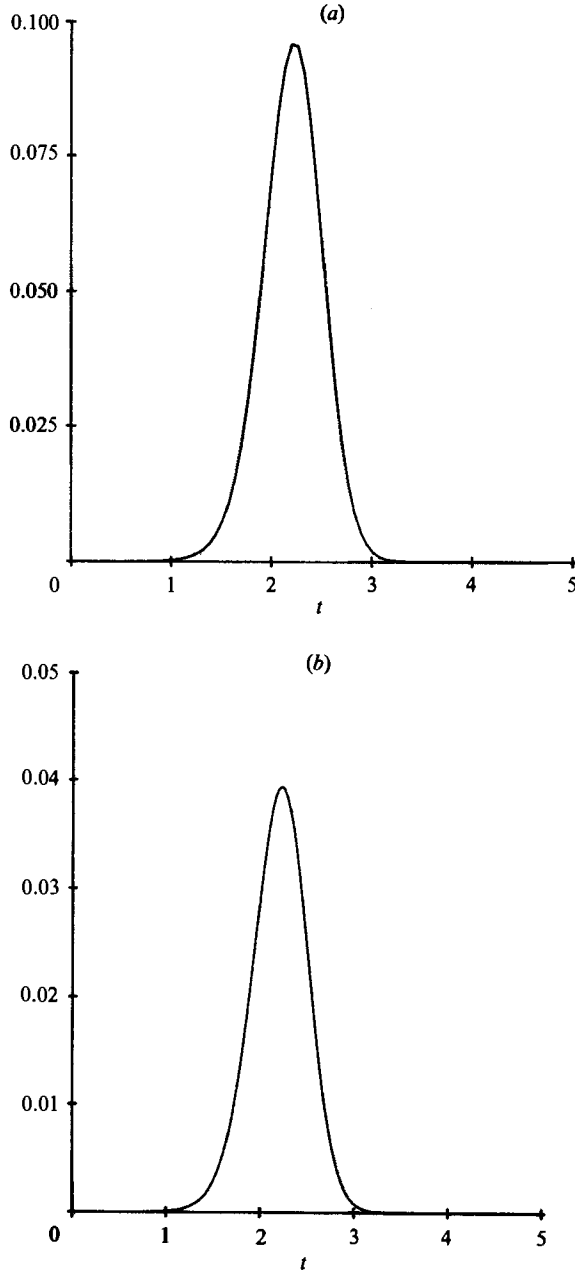


FIGURE 6. (a) Steadily oscillating Taylor-vortex flow at $\eta = 0.88$, $\alpha = 3.13$, $\overline{Re}_1 = 100$, $\epsilon_1 = 0.5$, $\gamma_1 = 0.79$: plot of $u_r(x = 0.5, \zeta = 0)$. The source of potential vorticity in equation (2.2) is $-10^{-3} \sin \alpha \zeta$. Note that $Re_{10} = 120.5$. We used $N = 15$, $M = 4$, $N_T = 800$. (b) As (a), but the vorticity source is at the inner cylinder wall, so that $\partial\psi/\partial x = 0.5 \times 10^{-3} \Delta t \eta(1 + \eta) \sin \alpha \zeta$ is the boundary condition.

initial-value code describes a perfect bifurcation scenario. The rather similar behaviour for the two rather different vorticity distributions supports the view that the observed behaviour may not be too dependent on the exact nature of the imperfection. We now used the first of our two models to study the frequency dependence of oscillations of amplitude $\epsilon_1 = 0.5$, to compare with the amplitude

equation model. At wavenumber $\alpha = 3.13$ and radius ratio $\eta = 0.88$ the critical steady-state Reynolds number is 120.5. With a source of vorticity of strength 10^{-3} we obtain an oscillating Taylor-vortex flow at $\overline{Re}_1 = 100$, as in figure 6. We found that $u_r(x = 0.5, \zeta = 0)$ reached a peak value of 0.414×10^{-2} during the cycle with $\omega_1 = 2$. At higher frequency, $\omega_1 = 4$, we obtained $u_r = 0.262 \times 10^{-3}$, a much lower value as expected from the §3 discussion. We introduce again the quantities used in the analysis of the amplitude equation: at $\overline{Re}_1 = 100$ we have

$$\frac{d\sigma}{dRe_1} = 0.212, \quad \mu = \frac{d\sigma}{dRe}(\overline{Re}_1 - Re_{10}) = -4.346, \quad \epsilon = \frac{d\sigma}{dRe_1} \overline{Re}_1 \epsilon_1 = 10.6, \\ A = 3.355.$$

In §3 we concluded that when $\mu < 0$ and the imperfections are such that the vortices do not reach $O(1)$ during the cycle then the peak velocity is proportional to c and has frequency dependence $\omega_1^{\frac{1}{2}} \exp(\Delta/\omega_1)$. For $\omega_1 = 2$ and 4, this formula predicts a ratio of peak velocity of 14.7, which is in fair agreement with the ratio 15.8 found by the initial-value code. We also ran the case $\omega_1 = 4$ with a vorticity source $c = 10^{-2}$ and obtained a velocity amplitude ten times larger than in the $c = 10^{-3}$ case. We conclude that the vorticity sources in the initial-value code give results very similar to those of the imperfect amplitude equation.

We can now proceed to study the development of the flow after the onset. All the following results have been obtained by means of the initial-value code described in §2, without the source of vorticity mentioned above. We consider a series of experiments of Ahlers which were performed at $\eta = 0.75$ and $\omega_1 = 4.0$; Ahlers defined the Reynolds numbers as

$$\left. \begin{aligned} Re_1(t) &= Re_{10}(1 + \epsilon_0 + \delta \sin(\omega_1 t)), \\ Re_2(t) &= 0, \end{aligned} \right\} \quad (4.9)$$

so that ϵ_0 is a measure of the distance from the steady onset. The connection to the previous notation (4.1) is that $\overline{Re}_1 = Re_{10}(1 + \epsilon_0)$ and $\epsilon_1 = Re_{10} \delta / \overline{Re}_1$.

In a first experiment Ahlers chose $\epsilon_0 = 0.1$ and $\delta = 0.4$ and measured the axial component of the velocity $u_z(t)$ at some point close to the inner cylinder as a function of time. Then $u_z(t)$ was analysed in Fourier modes

$$u_z = u_z^{(1)} \sin(\alpha \zeta) + u_z^{(2)} \sin(2\alpha \zeta) + u_z^{(3)} \sin(3\alpha \zeta) \dots,$$

where α is the dimensionless axial wavenumber. The results for the first Fourier component $u_z^{(1)}(t)$ as a function of time are the circles in figure 7. Note that $u_z^{(1)}$ is normalized by $u_{z0}^{(1)}/\epsilon_0^{\frac{1}{2}}$, where $u_{z0}^{(1)}$ is the first Fourier component of the velocity u_{z0} when there is no modulation. We have calculated $u_z(t)$ at the point $x = 0.1$ and $\zeta = 0.125\lambda$ by means of our initial-value program: the result for $u_z^{(1)}(t)$, normalized in the same way as Ahlers, is the solid line of figure 7: the agreement with Ahlers' experiment is good.

We next want to compare our computation and Ahlers' data to the result of the direct numerical integration of the amplitude equation. We have already learned how to identify μ , ϵ , ω , A and c in (3.2) and we have already seen that in Ahlers' experiments at $\epsilon_0 = 0.1$ and $\eta = 0.75$ we have $d\sigma/dRe = 0.31$. At steady Reynolds number $Re_1 = \overline{Re}_{10}(1 + \epsilon_0) = 94.3539$ we find $u_z = -3.56$ at the test point $x = 0.1$ and $\zeta = 0.125\lambda$, which we use for comparison to experiment. At this value of Re_1 , $A = \mu^{\frac{1}{2}} = 0.31(\overline{Re}_1 - \overline{Re}_{1c})^{\frac{1}{2}} = 1.63$, so the value of the constant which connects A to u_z via $A = ku_z$ is $k = -0.46$ for comparison to this experiment. Finally we assume $c = 0$

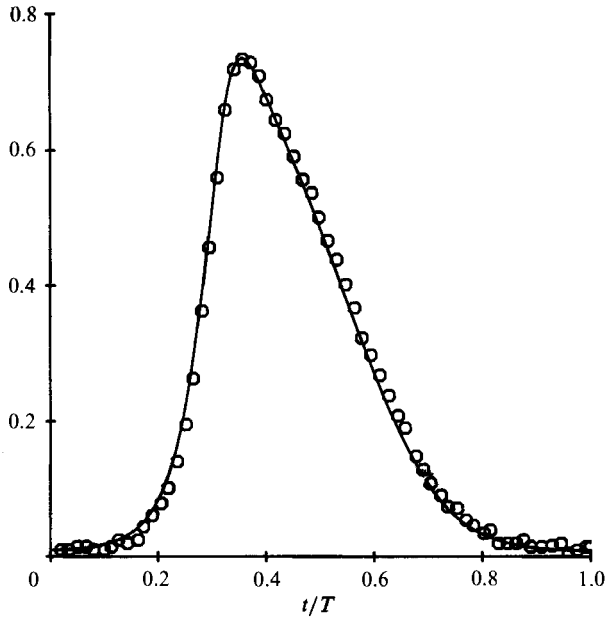


FIGURE 7. Comparison with the experiment of Ahlers (1988, private communication) at $\eta = 0.75$, $\omega_1 = 4$ with $\epsilon_0 = 0.1$ and $\delta = 0.4$. Plot of the first Fourier component $u_z^{(1)}(t)$ vs. t/T , normalized as described in the text: circles, experimental data; solid curve, result of the initial-value code with $\alpha = 3.13$, $N = 15$, $M = 6$, and $N_T = 800$.

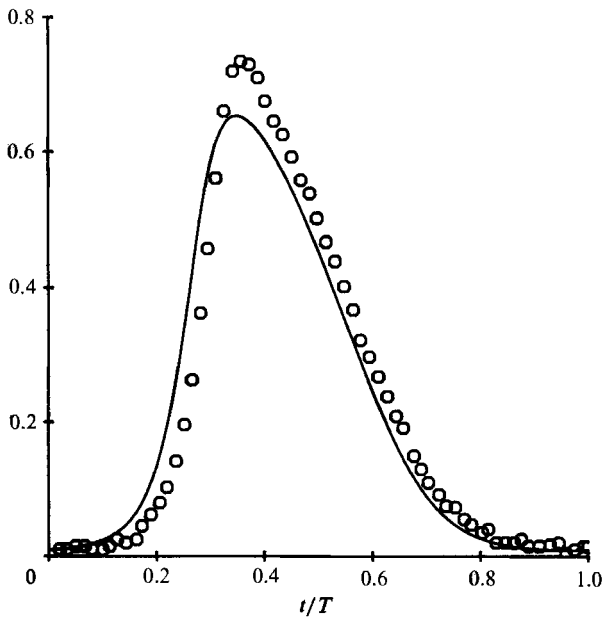


FIGURE 8. Comparison between the experimental data of Ahlers of figure 7 and the integration of the amplitude equation (3.2) with $\mu = 2.6463$, $\epsilon = 10.5854$, $\omega = 4$ and $c = 0$. The solution of the amplitude equation has been normalized as described in the text.

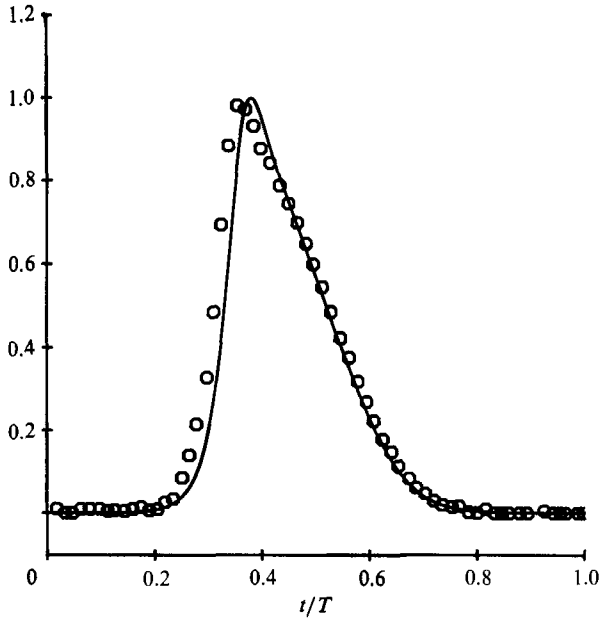


FIGURE 9. Comparison with the experiment of Ahlers (1988, private communication) at $\eta = 0.75$ with $\epsilon_0 = 0.1$, $\delta = 0.7$ and $\omega_1 = 4$. Plot of the first Fourier component $u_z^{(1)}(t)$ vs. t/T , normalized as described in the text: circles, experimental data; solid curve, result of the initial-value code with $\alpha = 3.13$, $N = 15$, $M = 6$ and $N_T = 800$.

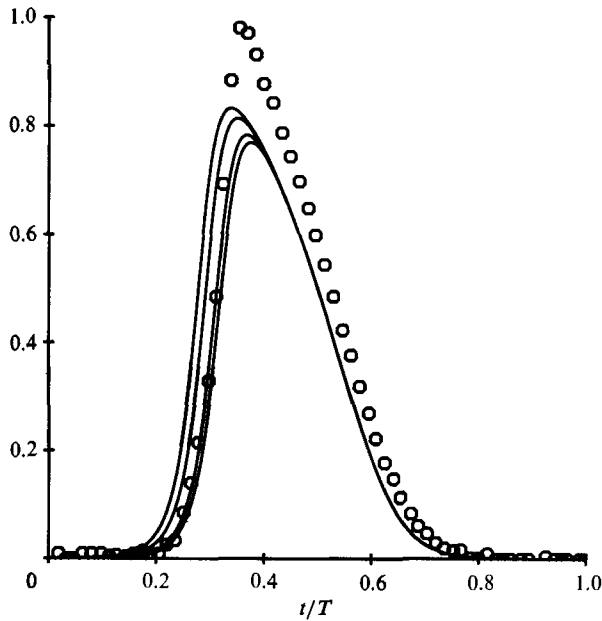


FIGURE 10. Comparison between the experimental data of Ahlers of figure 9 and the integration of the amplitude equation (3.2) with $\mu = 2.6464$, $\epsilon = 18.5234$, $\omega = 4$ and $c = 0, 0.001, 0.005$ and 0.01 ; the higher the value of c the earlier the amplitude rises. The solution of the amplitude equation has been normalized as described in the text.

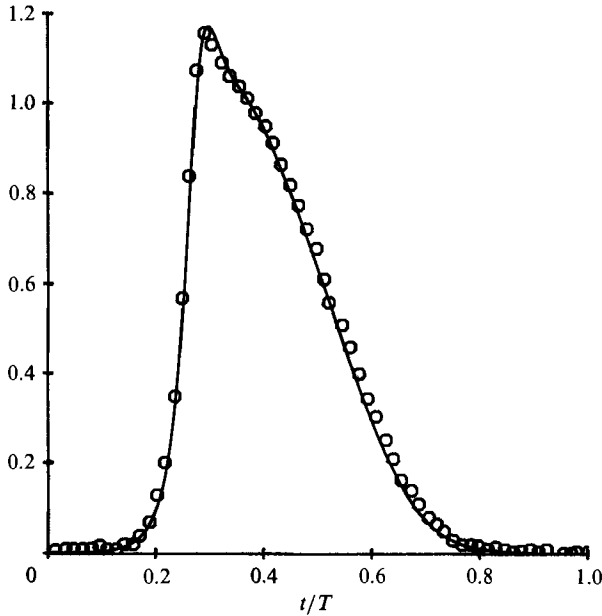


FIGURE 11. Comparison with the experiment of Ahlers (1988, private communication) at $\eta = 0.75$ with $\epsilon_0 = 0.2$, $\omega = 4$ and $\delta = 0.7$. Plot of the first Fourier component $u_z^{(1)}(t)$ vs. t/T , normalized as described in the text: circles, experimental data; solid curve, result of the initial-value code with $\alpha = 3.13$, $N = 15$, $M = 6$ and $N_T = 800$.

because we do not expect that in Ahlers' experiment at $\omega = 4$ the imperfections play a role as significant as they did in Walsh & Donnelly's (1988*a*) experiment where the frequency went down to $\omega = 0.48$. We have seen at the end of §3 that if $\mu > 0$ and $c \ll c_+$ the effect of the noise is insignificant: in the case of Ahlers' first experiment we obtain $c_+ \approx 0.12$ which is bigger than the typical value $c = 10^{-3}$. The result of the numerical integration of the amplitude equation is shown in figure 8 together with Ahlers' measurements: it does reproduce the general feature of the experimental data and it fails only to describe the region close to the peak.

In a second experiment at the same frequency $\omega_1 = 4$ and radius ratio $\eta = 0.75$ Ahlers chose the parameters $\epsilon_0 = 0.1$ and $\delta = 0.7$, i.e. the same relative distance from the onset of steady vortices but a larger modulation amplitude. The comparison between the data and our initial-value code is shown in figure 9. Note how the spike which develops at the maximum of the velocity is well reproduced. However the measured signal rises earlier than the calculated signal. We again attribute this discrepancy to the effect of the imperfections in the system. At this larger $\delta = 0.7$, imperfections become more important than in the previous $\delta = 0.4$ case: we find that c_+ is reduced and is $\approx 0.003 \approx c = 10^{-3}$. We have also computed the solution of the amplitude equation for increasing values of the imperfection c , shown in figure 10. Although the shape of the curve is not so well reproduced by the amplitude equation as by the full code, we see that a non-zero but small value of c is enough to make the solution to rise earlier, as in the experimental data.

In a third experiment, at the same frequency and radius ratio, Ahlers used the parameters $\epsilon_0 = 0.2$ and $\delta = 0.7$: the flow is modulated with the same amplitude but is further away from the critical Reynolds number. In this case we expect the modulated vortex to be more distorted, being driven at higher Reynolds number,

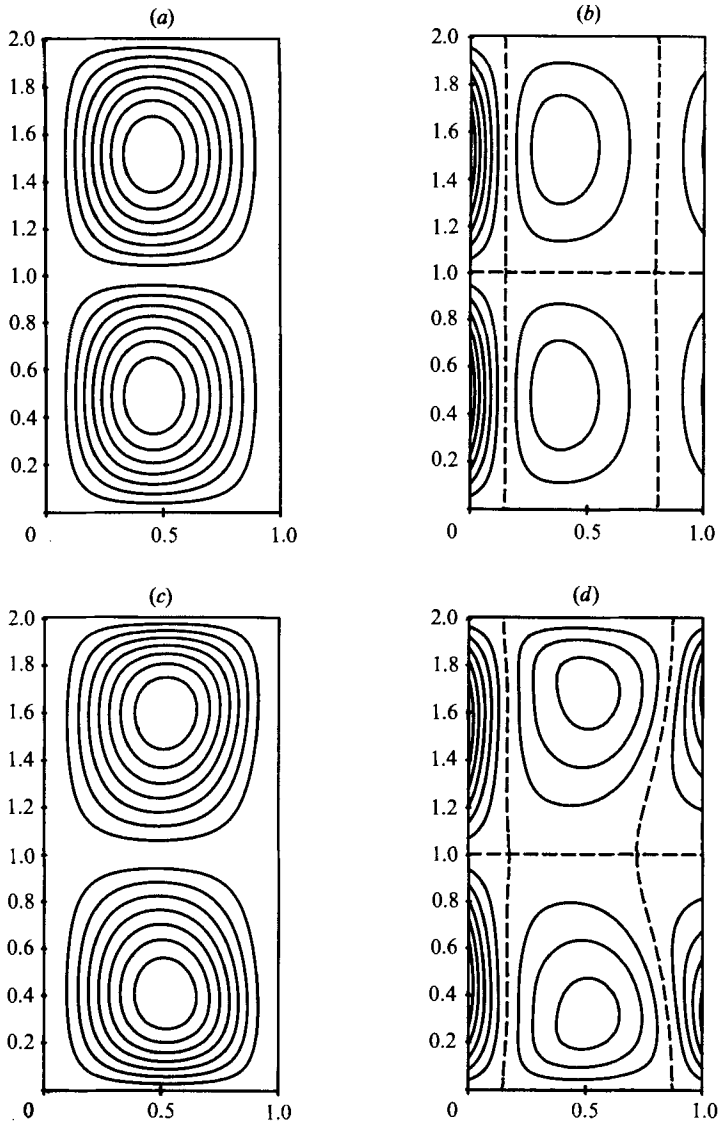


FIGURE 12. Plot of the streamlines ψ and modified azimuthal vorticity Z calculated by our initial-value code for the case of figure 11; for the streamlines contours are spaced at $\Delta\psi = \frac{1}{8}\psi_{\max}$, and for Z contours are spaced at $\Delta Z = \frac{1}{8}Z_{\max}$. (a) at time $t/T = 0.20$ contours of ψ , $\psi_{\max} = 0.37$. (b) $t/T = 0.20$ contours of Z , $Z_{\max} = 29.6$. (c) $t/T = 0.295$ contours of ψ , $\psi_{\max} = 5.63$. (d) $t/T = 0.295$ contours of Z , $Z_{\max} = 337.3$.

and that the imperfections play a less important role as $c_+ = 0.01$ is bigger than c . Figure 11 shows how the experimental data agree with the initial-value code. As we expect, the theoretical curve and the data rise at the same point in the cycle, confirming that imperfections are not significant in this case.

It is interesting to study how the flow varies during a cycle: in figure 12 we show the streamlines and the lines of equal vorticity at different times during an oscillation for Ahlers' experiment at $\epsilon_0 = 0.2$ and $\delta = 0.7$: figures 12(a) and 12(b) show the streamlines and vorticity at $t/T = 0.2$, when the amplitude is small, and 12(c) and 12(d) give the corresponding pictures at $t/T = 0.295$, near maximum amplitude. The

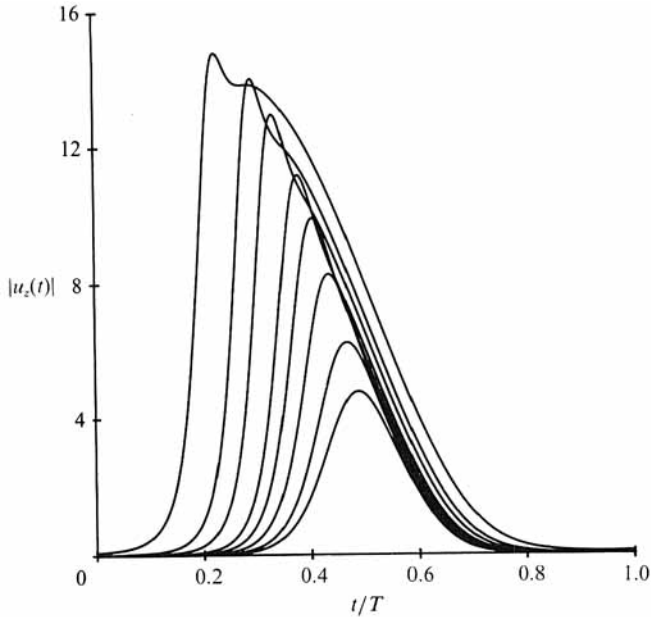


FIGURE 13. Plot of $|u_z(t)|$ vs. t/T computed for the case of figure 12, $\eta = 0.75$, $\omega_1 = 4$ and $\delta = 0.7$ at the test point $x = 0.1$ and $\zeta = 0.125\lambda$, at increasing values of $\epsilon_0 = 0.01, 0.025, 0.050, 0.075, 0.10, 0.15, 0.20$ and 0.30 . We used $N = 15$, $M = 6$ and $N_T = 800$.

most interesting feature is that the core of the Taylor vortex moves towards the outflow region of the cell pair when the velocity is at the highest value. It is then not surprising that the amplitude equation fails to describe the region close to where $u_z(t)$ is maximum, because its derivation assumes that the spatial dependence is the same during the cycle. The movement of the vortex core also explains why the shape of the function $u_z(t)$ develops a sharp peak: $u_z(t)$ is measured or calculated at a fixed point near the inner cylinder in the outflow region; when the vortex is at the maximum strength it becomes distorted in such a way as to increase the value of the velocity at that fixed point, an effect that is not reproduced by the amplitude equation. In figure 13 we show a series of plots of $u_z(t)$ for various values of ϵ_0 at the same $\delta = 0.7$ to show how the peak of $u_z(t)$ develops and becomes distorted.

If one considers the value of the average of u_z^2 one finds that this is proportional to ϵ_0 at fixed modulation δ , as shown in figure 14: this verifies the Landau amplitude law for modulated flow. Note that the curve joining the circles (modulated flow) does not pass through the origin because of the threshold shift. Indeed, the threshold shift could in principle be measured by finding the intercept at $u_z^2 = 0$: this was the idea in Donnelly's (1964) experiment, but unfortunately the presence of the transient vortices made it difficult to obtain accurate results by this approach.

Finally we consider the case in which it is the outer cylinder that is modulated, the subject of an experiment of Walsh & Donnelly (1988*b*). In the experiment at first the outer cylinder was held fixed and the inner cylinder was rotated at constant Reynolds number $Re_1 = \bar{Re}_1 > Re_{10}$ so as to produce a steady Taylor-vortex flow. Then the experimentalists discovered that if the modulated the outer cylinder at Reynolds number $Re_2(t) = \epsilon_2 \bar{Re}_1 \sin(\omega_2 t)$ the vortices disappeared and the flow returned into the Couette state. The conclusion is that the modulation of the outer cylinder strongly stabilizes the flow, contrary to what happens for modulations of the

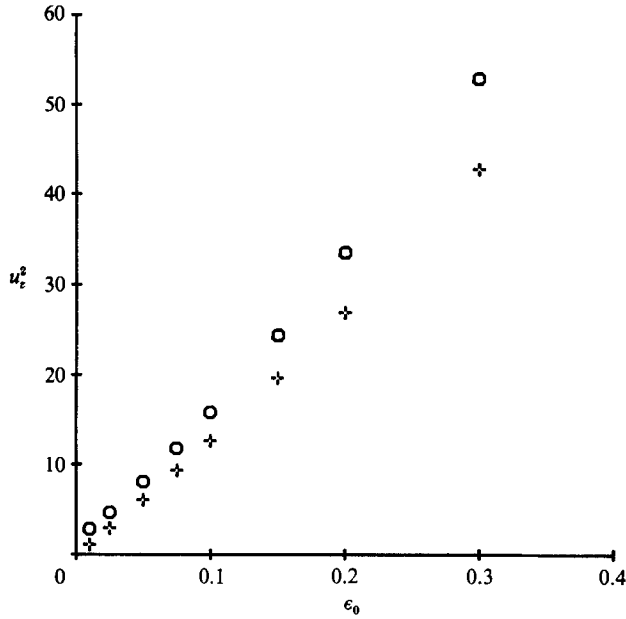


FIGURE 14. Circles, time average of u_z^2 calculated by our initial-value code for the case of figure 10 at $\eta = 0.75$, $\omega_1 = 4$ and $\delta = 0.7$ at the test point $x = 0.1$ and $\zeta = 0.125\lambda$; crosses, corresponding steady-state value of u_z^2 . We used $N = 15$, $M = 6$ and $N_T = 800$.

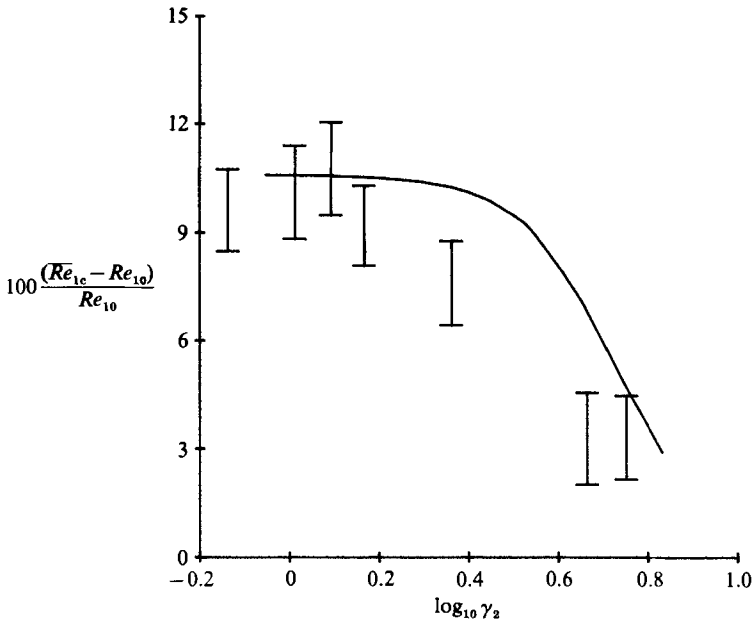


FIGURE 15. Comparison with Walsh & Donnelly's experiment (1988*b*) at $\eta = 0.88$, $\epsilon_2 = 0.5$. We plot the threshold shifts $100(\overline{Re}_{1c} - Re_{10})/Re_{10}$ vs. $\log_{10} \gamma_2$; bars, experimental points; solid line, our calculations with $\alpha = 3.13$, $N = 15$, and $N_T = 1000$.

inner cylinder. Figure 15 shows the comparison of our Floquet theory with this experiment: we plot threshold shifts as a function of frequency (actually r against $\log_{10} \gamma_2$) at $\epsilon_2 = 0.5$ and $\eta = 0.88$. The agreement with the experiments is reasonable. It is interesting to compare this stabilization with the destabilization shown in the

solid curve of figure 2: recall that in figure 2 the data for the solid curve were multiplied by a factor of 10, so that at low frequency r is about -0.8% , whereas in figure 17 the change in r at low frequency is about 8% . Because the shift is much larger when the outer, rather than the inner, cylinder is modulated, the experiment is easier and the results in better agreement with the theory. The reason why modulation stabilizes in this case is straightforward to understand: Taylor (1923) showed that as Ω_2 is varied at fixed Ω_1 in the steady-state problem, the marginal curve has a U-shape: that is the flow becomes more stable whether Ω_2 is positive or negative. We therefore expect this type of modulation to be stabilizing.

5. Conclusions

Both the experiments and the theory of the primary bifurcation in modulated Couette flow have presented a rather confused picture in the past, but a clearer view is beginning to emerge. For modulation of the inner cylinder about a non-zero mean, the threshold shift of the critical Reynolds number is quite small, and is close to the experimentally observable limit with modern apparatus. The early experiments of Donnelly were not sufficiently accurate to find this small effect, and subsequent workers have found a negative threshold shift, rather than Donnelly's positive value. There was, however, nothing wrong in principle with Donnelly's method of determining the critical Reynolds number, but the presence of transient vortices due to imperfections made it difficult to get accurate results.

Some of the more recent experiments have apparently erred in the opposite direction: negative threshold shifts have been found (corresponding to modulation being destabilizing), as predicted by Hall, but their magnitude has been much too large, particularly at low frequency. We believe, however, that the explanation given in this paper, namely that small imperfections can give rise to large-amplitude vortices below the critical Reynolds number, can account for the discrepancies. Experiments with higher frequencies, such as Ahlers' laser-Doppler observations, are in reasonable agreement with the theory, as are the experiments in which the outer cylinder is modulated, the threshold shift being then much larger.

We also believe that an important source of confusion, both for experimentalists and theoreticians, has been the nature of the low-frequency limit. The 'physically intuitive' idea that at low frequencies the system must be unstable if the instantaneous Reynolds number exceeds the steady critical Reynolds number at any time during the cycle is only true if there are imperfections in the system. In the theoretical perfect bifurcation the critical Reynolds number in the low-frequency limit is completely different from this physically intuitive value. This behaviour is quite common in systems with two small parameters, here the frequency ω and the degree of imperfection c ; the physically intuitive critical Reynolds number comes from first letting $\omega \rightarrow 0$ and then letting $c \rightarrow 0$, whereas in the perfect bifurcation analysis we first send $c \rightarrow 0$ and then let $\omega \rightarrow 0$. The value of \bar{Re}_{1c} obtained depends on the order in which the limits are taken.

The amplitude equation gives a qualitatively correct description of the behaviour near transition, although the full time-step integration procedure gives a much more accurate reproduction of the time-dependence of the amplitude: this is because the numerical simulation takes into account the changing shape of the vortex pattern throughout the cycle. It is also possible to make analytical progress with the imperfect amplitude equation and hence to see directly the effect of imperfection on the disturbance, and how this depends on the parameters. This makes it possible to

develop criteria for the importance of imperfections; criteria that seem to be reasonably successful in interpreting the experiments. We have also been able to model the imperfections in the initial-value code by including a source of vorticity: a steadily oscillating ‘transient’ vortex can then be produced at subcritical Reynolds number.

On the theoretical side, our calculations agree with those of Hall and Kuhlmann *et al.* and disagree with those of Carmi & Tustaniwskyj. The most likely source of this disagreement has been identified.

We gratefully acknowledge access to unpublished experimental data from Professor G. Ahlers, Professor R. J. Donnelly, and Mr T. J. Walsh. Dr C. F. Barenghi acknowledges support from SERC grant GR/D/30433.

REFERENCES

- AHLERS, G., CROSS, M. C., HOHENBERG, P. C. & SAFRAN, S. 1981 The amplitude equation near the convective threshold: application to time-dependent heating experiments. *J. Fluid Mech.* **110**, 297–334.
- AHLERS, G., HOHENBERG, P. C. & LÜCKE, M. 1985*a* Thermal convection under external modulation of the driving force. I. The Lorenz model. *Phys. Rev. A* **32**, 3493–3518.
- AHLERS, G., HOHENBERG, P. C. & LÜCKE, M. 1985*b* Thermal convection under external modulation of the driving force. II. Experiments. *Phys. Rev. A* **32**, 3519–3534.
- BENJAMIN, T. B. 1978*a* Bifurcation phenomena in steady flow of a viscous fluid. I. Theory. *Proc. R. Soc. Lond. A* **359**, 1–26.
- BENJAMIN, T. B. 1978*b* Bifurcation phenomena in steady flow of a viscous fluid. II. Experiments. *Proc. R. Soc. Lond. A* **359**, 27–43.
- BHATTACHARJEE, J. K., BANERJEE, K. & KUMAR, K. 1986 Modulated Taylor–Couette flow as a dynamical system. *J. Phys. A: Math. Gen.* **19**, L835–L839.
- CARMI & TUSTANIWSKYJ, J. I. 1981 Stability of modulated finite-gap cylindrical Couette flow: linear theory. *J. Fluid Mech.* **108**, 19–42.
- CROSS, M. C., HOHENBERG, P. C. & LÜCKE, M. 1983 Forcing of convection due to time-dependent heating near threshold. *J. Fluid Mech.* **136**, 269–276.
- DANIELS, P. G. 1977 The effect of distant sidewalls on the transition to finite amplitude Bénard convection. *Proc. R. Soc. Lond. A* **358**, 173–197.
- DAVIS, S. H. 1976 The stability of time-periodic flows. *Ann. Rev. Fluid Mech.* **8**, 57–74.
- DOMINGUEZ-LERMA, M. A., AHLERS, G. & CANNELL, D. S. 1985 Effects of ‘Kalliroscope’ flow visualisation particles on rotating Couette–Taylor flow. *Phys. Fluids* **28**, 1204–1206.
- DONNELLY, R. J. 1964 Experiments on the stability of viscous flow between rotating cylinders. III. Enhancement of stability by modulation. *Proc. R. Soc. Lond. A* **781**, 130–139.
- DONNELLY, R. J., REIF, F. & SUHL, H. 1962 Enhancement of hydrodynamic stability by modulation. *Phys. Rev. Lett.* **9**, 363–365.
- FINUCANE, R. G. & KELLY, R. E. 1976 Onset of instability in a fluid layer heated sinusoidally from below. *Intl J. Heat Mass Transfer* **19**, 71–85.
- HALL, P. 1975 The stability of unsteady cylinder flows. *J. Fluid Mech.* **67**, 29–63.
- HALL, P. 1983 On the nonlinear stability of slowly varying time-dependent viscous flows. *J. Fluid Mech.* **126**, 357–368.
- HALL, P. & WALTON, I. C. 1979 Bénard convection in a finite box: secondary and imperfect bifurcation. *J. Fluid Mech.* **90**, 377–395.
- HEINRICHS, R. M., CANNELL, D. S., AHLERS, G. & JEFFERSON, M. 1988 Experimental test of the perturbation expansion for the Taylor instability at various wavevectors. *Phys. Fluids* **31**, 250–255.
- HSIEH, D. Y. & CHEN, F. 1984 On a model study of Couette flow. *Phys. Fluids* **27**, 321–322.
- JONES, C. A. 1985 Numerical methods for the transition to wavy Taylor vortices. *J. Comput. Phys.* **61**, 321–344.

- KUHLMANN, H. 1985 Model for Taylor–Couette flow. *Phys. Rev. A* **32**, 1703–1707.
- KUHLMANN, H., ROTH, D. & LÜCKE, M. 1989 Taylor vortex flow under harmonic modulation of the driving. *Phys. Rev. A* **39**, 745–762.
- LETTIS, D. S. L. 1986 The stability of time dependent fluid flows. Ph.D. thesis, University of Exeter.
- MARCUS, P. 1984 Simulation of Taylor–Couette flow. Part 1. Numerical methods and comparison with experiment. *J. Fluid Mech.* **146**, 45–64.
- NIEMELA, J. J. & DONNELLY, R. J. 1987 External modulation of Rayleigh–Bénard convection. *Phys. Rev. Lett.* **59**, 2431–2434.
- PARK, K., BARENGHI, C. F. & DONNELLY, R. J. 1980 Subharmonic destabilization of Taylor vortices near an oscillating cylinder. *Phys. Lett.* **78A**, 152–154.
- RILEY, P. J. & LAURENCE, R. L. 1976 Linear stability of modulated circular Couette flow. *J. Fluid Mech.* **75**, 625–646.
- RILEY, P. J. & LAURENCE, R. L. 1977 Energy stability of modulated circular Couette flow. *J. Fluid Mech.* **79**, 535–552.
- SCHAEFFER, P. G. 1980 Qualitative analysis of a model for boundary effects in the Taylor problem. *Math. Proc. Camb. Phil. Soc.* **87**, 307–337.
- SEMINARA, G. & HALL, P. 1976 Centrifugal instability of a Stokes layer: linear theory. *Proc. R. Soc. Lond. A* **350**, 299–316.
- SEMINARA, G. & HALL, P. 1977 Centrifugal instability of a Stokes layer: nonlinear theory. *Proc. R. Soc. Lond. A* **354**, 119–126.
- TAYLOR, G. I. 1923 Stability of a viscous liquid contained between two rotating cylinders. *Phil. Trans. R. Soc. Lond. A* **223**, 289–343.
- THOMPSON, R. 1969 Instabilities of some time-dependent flows. Ph.D. thesis, Department of Meteorology, Massachusetts Institute of Technology.
- TUSTANIWSKYJ, J. I. & CARMÍ, S. 1980 Nonlinear stability of modulated finite gap Taylor flow. *Phys. Fluids* **23**, 1732–1739.
- WALSH, T. J. 1988 The influence of external modulation on the stability of azimuthal Taylor–Couette flow: an experimental investigation. Ph.D. thesis, University of Oregon.
- WALSH, T. J. & DONNELLY, R. J. 1988*a* Stability of modulated Couette flow. *Phys. Rev. Lett.* **58**, 2543–2546.
- WALSH, T. J. & DONNELLY, R. J. 1988*b* Couette flow with periodically corotated and counterrotated cylinders. *Phys. Rev. Lett.* **60**, 700–703.